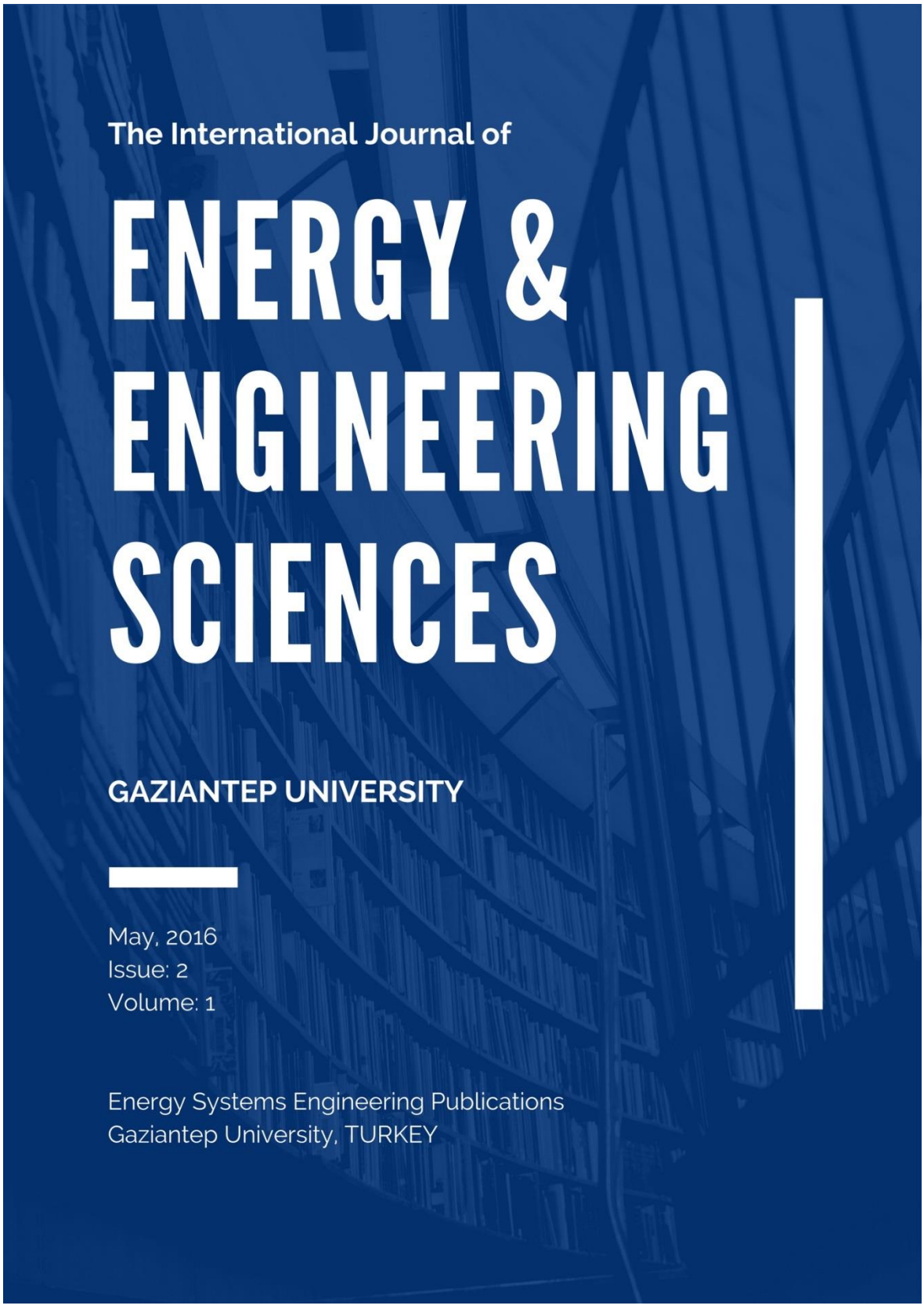
The International Journal of
ENERGY & ENGINEERING SCIENCES
GAZIANTEP UNIVERSITY
May, 2016
Issue: 2
Volume: 1
Energy Systems Engineering Publications
Gaziantep University, TURKEY

Gaziantep University Engineering Faculty
+90 342 360 12 00
+90 342 360 10 13
gaziantep.university.ijees@gmail.com
https://uemk-conferences.wixsite.com/ijees

Published by

Gaziantep university, Engineering Faculty, Energy Systems Engineering,
Üniversite Bulvarı 27310 Şehitkamil - Gaziantep, TÜRKİYE

ISSN

Table of Contents

MICROCONTROLLER-BASED COOLING OF A SINGLE-PHASE TRANSFORMER WITH THERMOELECTRIC MODULE

Adem DALCALI
Electrical-Electronics Engineering, Karabük University
ademdalcali@karabuk.edu.tr

Hüseyin DEMIREL
Electrical-Electronics Engineering, Karabük University
hdemirel@karabuk.edu.tr

Emre CELIK
Electrical-Electronics Engineering, Gazi University
emrecelik@gazi.edu.tr

ABSTRACT: Copper and core losses produced in the windings and core of a transformer cause the transformer to heat up, thereby deteriorating the transformer performance. The resulting heat needs to be thrown away out of the machine as it is more likely to damage either machine itself or its equipment, or both. For this aim, a new cooling technique for transformer core and windings, which is a unique one in its field related to transformer cooling systems, is presented in this paper using the peltier effect of thermoelectric module. In the several tests carried out, an industrial type single-phase transformer is heated by a certain amount under various operating conditions. Thanks to the presented technique, the transformer heat has been successfully kept within a predefined temperature band. Other than single-phase transformers, the presented technique can be easily applied for cooling of three-phase transformers as well. Due to its ease of application, simple structure and low cost, the presented technique is a powerful alternative to other existing techniques in the literature.

Key words: transformer cooling, temperature control, thermoelectric module, peltier effect

INTRODUCTION

During the design phase of a transformer, optimal design for each stage in solutions of electromagnetic, thermal and mechanical problems is required to achieve. As soft magnetic materials forming the transformer core constitute the magnetic circuitry of the machine, these materials are expected to have the following characteristic features; high permeability to reduce the magnetic circuit reluctance, high saturation property to reduce the volume and weight of the iron in addition to lower iron losses which give rise to increase in machine temperature (Gürdal, 2015). Copper losses produced in the windings and iron losses in

ferromagnetic core under the effect of time-varying magnetic field release heat in the windings and magnetic core of the machine, respectively. By transferring the released heat into the external environment, winding temperature needs being reduced as much as possible. In this way, more current of the desired magnitude can pass through the same conductor cross-section and it is also possible to avoid the saturation flux density that decreases with temperature.

Büyükbıçakcı developed an alternative approach to the transformer cooling methods using a phase shifter material. As a result of the experiments carried out, it is shown that the utilized material cooled the heated points of the transformer at the same time and succeeded in keeping them in a certain temperature value (Büyükbıçakçı, 2006). In the literature, there are many applications that have been performed using both effects of thermoelectric material (Aly & Al-Lail, 2006; Yu et al., 2012; Liu et al., 2007; Vinoth & Prema, 2014; Hsu et al., 2013). Çicek and et.al carried out the design and implementation of a blood transport container and expressed that it is possible to carry the medical samples without any distortion (Çicek et al., 2010). Demirel identified a close relationship between the temperatures of brain and other parts in the hypothermia system which was modeled with artificial neural networks and implemented based upon the microcontroller (Demirel,2010). Tan, in his thesis, carefully examined the system performance and temperature values upon the processor and motherboard belonging to a server using heat spreader, water cooling system and thermoelectric cooler (TEC), which is called as Peltier. After performing several tests by means of software for each cooling system, he identified that the most effective cooling method came out to be the TEC while the server was continuously under the workload (Tan, 2013). Chein and Chen analyzed the thermoelectric cooling system theoretically and experimentally to make the tank cooling, which was full of water. According to the test results, they found that the tank temperature decreased over time (Chein & Chen, 2005). Demirel and et.al conducted a test system that computed the characteristic parameters of the thermoelectric modules under dissimilar thermal loads (Demirel et al., 2007).

Although the cooling operation in rotating machines are performed by inherent air currents, in transformers which have no rotating parts, it can be done in various ways such as via air, oil and water. In this paper, a unique cooling system based on microcontroller has been developed by taking advantage of the peltier effect of thermoelectric module

Experiments have been carried out for different secondary currents using both single and dual thermoelectric modules. Cooling is performed by single module when Is is 3 A and 4 A, while two modules are used for a secondary current of 5 A because of the fact that single module could not be sufficient for cooling operation. In the successive experimental studies, good results are achieved. With this regard, the presented technique is a powerful alternative to other existing

techniques in the literature due to its ease of application, simple structure and low cost.

THERMOELECTRIC MODULE

Thermoelectric materials are the elements whose terminals direct current (DC) electrical energy is obtained when forming a temperature difference between their two surfaces. On the other hand, they produce temperature difference when given DC energy to their connection terminals. We may mention about two effects upon the operation of thermoelectric modules. Firstly, it is the seebeck effect that generates electrical current with the principle of temperature difference between the surfaces. Secondly, it is the peltier effect that constitutes a temperature difference between the surfaces when a thermoelectric module is connected to a DC power supply (Ionescu et al., 2011; Wey, 2006; Shaojing & Qin, 2010).

Thermoelectric module is an element composed of P- and N-type semiconductors materials that are connected in series electrically and in parallel thermally. They have the upper and bottom surfaces covered by ceramic, and they also have a feature of working quite (Yalçınkaya, 2008; Kim et al., 2014; Carmo et al., 2011). If one ends of the two conductors having distinct self-resistance are combined with each other and a current is allowed to flow through these combined conductors, temperature of the one end is decreased while the other's is increased, in a manner that provides heat transfer from one to another. The resulting effect is called the peltier effect, and can be represented in Figure 1.

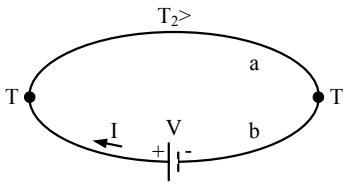

Figure 1. Peltier Effect

The amount of heat generated at the junction is proportional to the applied current and its definition per unit time can be expressed as in Eq. (1).

$$Q_p = \pi \cdot I \qquad (1)$$

where π is the peltier coefficient, Q_p is equal to the peltier heat stated in watts and I is the electrical current (Tan, 2013; Carmo et al., 2011; Dikmen, 2002; Lineykin et al., 2007; Martinez et al., 2012; Wang et al., 2012). The temperature difference between the two surfaces of a thermoelectric module can be given by Eq. 2

$$\Delta T = T_k - T_c \qquad (2)$$

In Eq. 2, T_k and T_c are the hot and cold surface temperatures of the thermoelectric module, respectively (Bulut, 2005). Heating and cooling effect coefficients (COP) of thermoelectric modules can be defined as in Eq. (3) and (4).

$$COP_k = Q_k / W_e \quad (3)$$

$$COP_c = Q_c / W_e \quad (4)$$

where COP_k is the heating and COP_c is the cooling effect coefficient.

THE DEVELOPED COOLING SYSTEM

The designed and implemented system is given in Figure 2. The developed control card, which consists of a PIC16F877A microprocessor, 12 V low-power relays and BC547 transistors for driving the TECs and fan, is seen in Figure 2(a). Figure 2(b) shows the cooling configuration where a typical single-phase transformer, TEC-12706 thermoelectric modules, LM35 temperature sensor, low-volume heat sink, and a small fan are used. The thermoelectric modules are located on the upper part of the transformer core underneath the heat sink. The cold side of the module is against the core, and the hot side is adjacent with the heat sink. Thermal paste is used in order to ensure thermal conductivity.

The transformer temperature is measured with LM35 placed between the transformer and the surrounding metal layer. This metal layer covers the surface of the transformer allowing the heat transmission from the windings to the core. Thus, when the cooling operation is enabled, the windings cooling from the core becomes faster. The exact temperature is compared to its reference within the microcontroller. As a result of this comparison, on/off state of the thermoelectric module and fan system are determined. If the temperature is higher than the reference, then the cooling system is activated and it is kept active until the temperature falls below the reference. Both fan and thermoelectric module are driven by the transistors and relays in the control card to isolate them from the microprocessor.

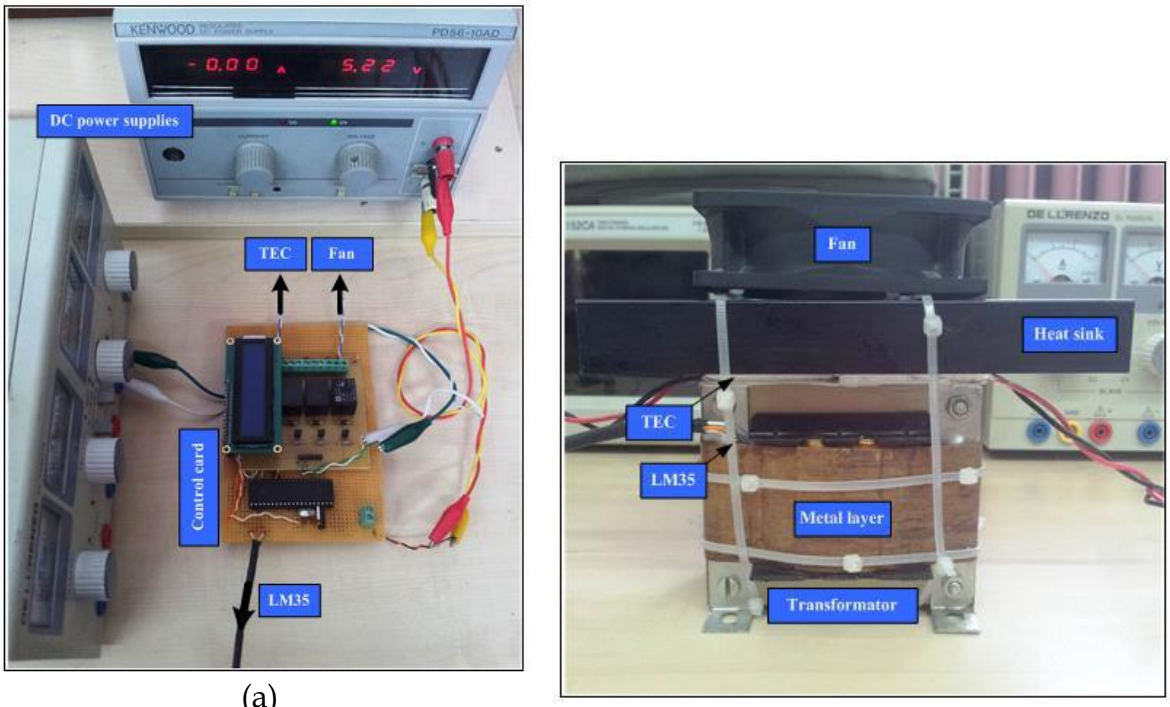

(a) (b)

Figure 2. The Experimental Setup (a) Control Card, (b) Cooling Configuration

The flowchart of the presented technique is given in Figure 3 where the microcontroller input-output pin adjustments, variable definitions, analog-digital converter settings, etc. are set firstly. Then, the transformer temperature is read by LM35, which is displayed on the LCD screen for operator knowledge. If the measured temperature is above 35 °C, the thermoelectric module and fan become active forthwith. Once the temperature drops below 35 °C, the thermoelectric module is deactivated. For the purpose of removing the resulting heat in the hot side of the thermoelectric module, fan operation is maintained for a while. As understood from the above explanations, the system operates like a hysteresis control, which is known as the simplest technique in control theory.

As for the loaded operating conditions of the corresponding transformer, short-circuit tests are performed under different current values where the primary voltage is increased until the secondary short-circuit current reaches the value up to the 125% times its rated current 4 A.

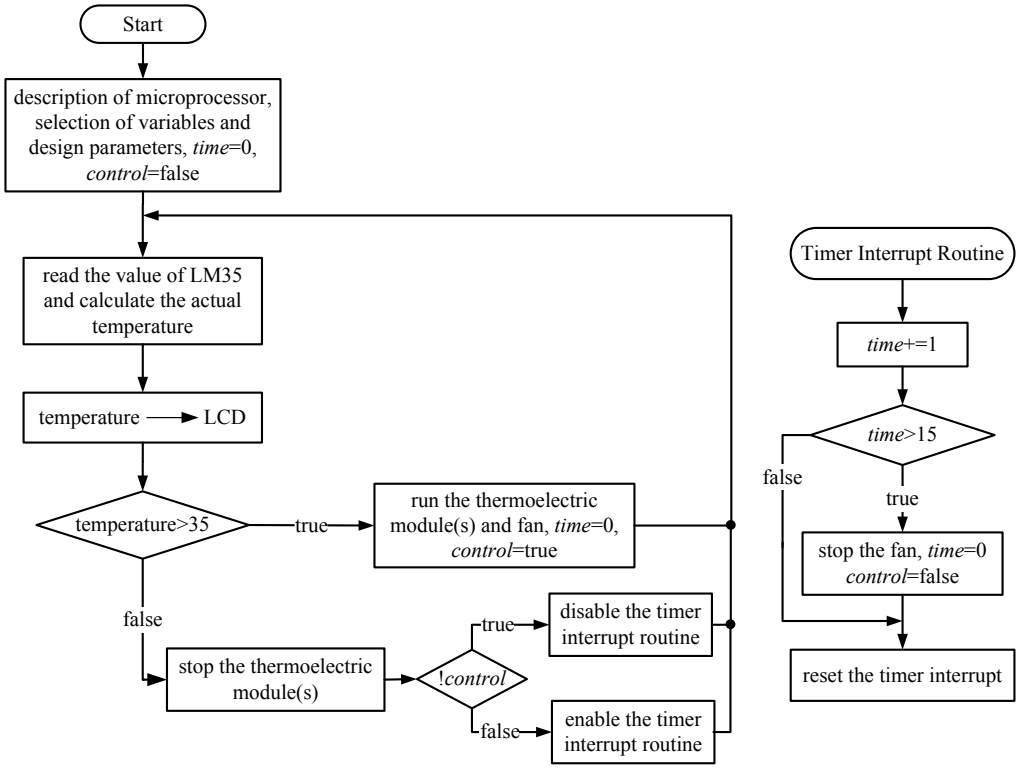

Figure 3. Flowchart of the Proposed System

Technical specifications of the thermoelectric module are reported in Table 1.

Table 1. Specifications of TEC-12706

Specifications	25 °C	50 °C
Q_{max} [W]	50	57
I_{max} [A]	6,4	6,4
V_{max} [V]	14,4	16,4
Δt_{max} [^{0}C]	66	75
Module Resistance [Ω]	1,98	2,3

In Table 1, Q_{max} is the maximum heat drawn from the cooling environment, and Δt_{max} is the highest temperature difference that can occur between the cooling surfaces.

EXPERIMENTAL RESULTS

In the experimental studies, supplying the transformer from variable AC power source, short-circuit tests are performed by taking the transformer secondary current I_s and primary voltage V_p into consideration. The secondary currents are set to 3 A, 4 A and 5 A, respectively. The obtained results using single TEC module is given in Figure 4 where I_s is 3 A. After a 39 minute period from the

beginning of the experiment, the transformer temperature raised over its reference temperature 35.2 ºC. In this case, the TEC module was activated and it could drop the temperature to 34.2 ºC in 15 seconds. When the temperature is above the reference, the temperature was again lowered successfully by making the TEC become active. In Table 2, TEC and fan currents and voltage measurements are given.

Table 2. TEC and Fan Measurements

	Current[A]	Voltage[V]	Power[W]
TEC	2,81	8,6	24,16
Fan	0,07	12,1	0,85

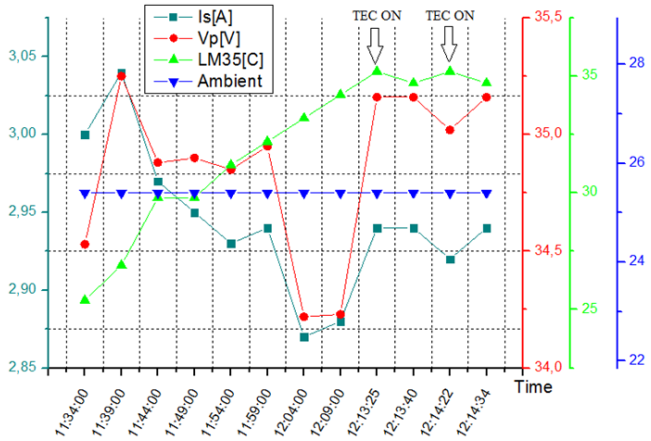

Figure 4. Experimantal Results When The Secondary Current Is 3A

In Figures 5-6, similar satisfactory experimental results are given when Is is 4 A and 5 A, respectively. In Figure 6, the experiment started at 14:03, and when the temperature reached to 35.2 ºC at 14:16:53, the TEC module was activated and it again dropped the temperature to 34.2 ºC in 22 seconds.

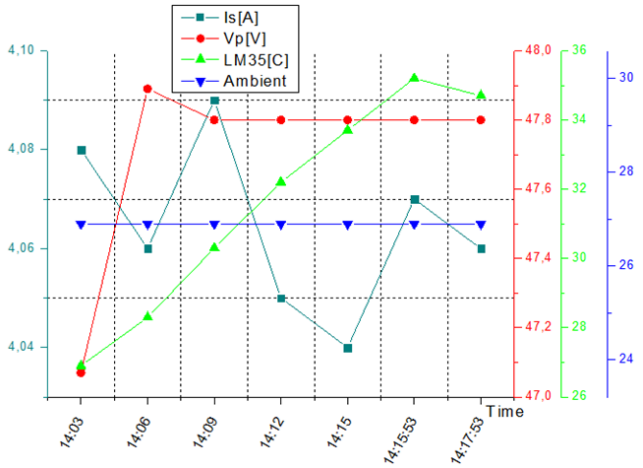

Figure 5. Experimantal Results When The Secondary Current Is 4A

In Figure 6, after 8 minutes from the beginning of the experiment, as the transformer temperature raised over the reference temperature 35.2 °C, the TEC module became active. However, in this operating condition, the temperature could not be reduced below the reference with single TEC module. In order to ensure adequate amount of cooling, one more TEC module was added to the experimental setup and the experiment was repeated under the same conditions. The obtained results with two TEC modules are promising and are given in Figure 7. In the new system with two TEC modules, the required cooling was provided and the temperature could be kept within the desirable range consistently. In Table 3, the current and voltage values of the fan, TEC1 and TEC2 modules are given when they are active.

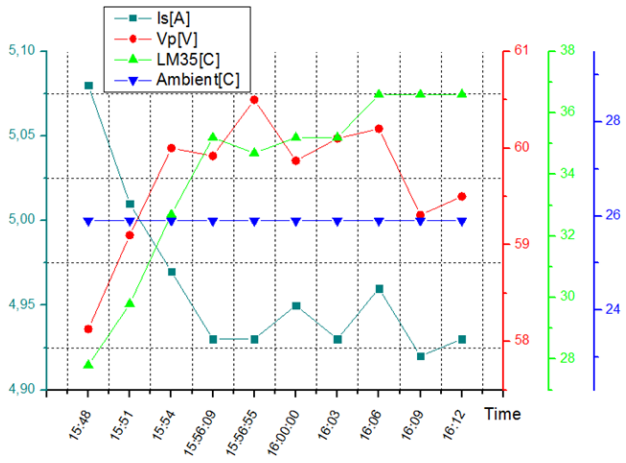

Figure 6. Experimantal Results When The Secondary Current Is 5A

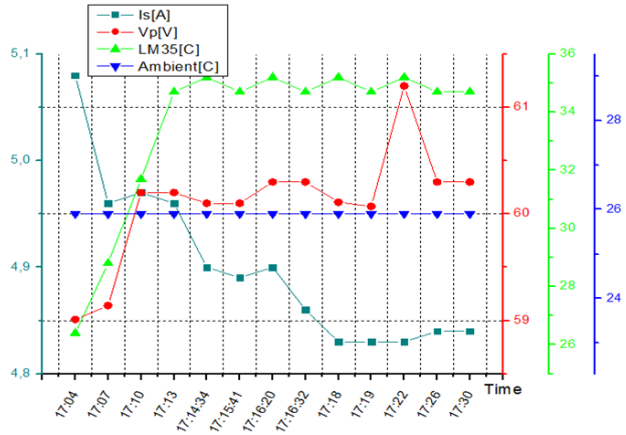

Figure 7. Experimantal Results When The Secondary Current Is 5A With Two TEC Modules

Table 3. Current and Voltage Values of the Fan, TEC1 and TEC2 Modules

	Current[A]	Voltage[V]	Power[W]
TEC1	2,92	9,1	26,57
TEC2	2,91	8,2	23,87
Fan	0,07	12,1	0,85

CONCLUSIONS

In this paper, a successful cooling scheme for transformer core and windings has been carried out using the peltier effect of thermoelectric module. According to the experimental results, the heat arisen due to the power losses could be ensured to efficiently remain within the certain range, protecting the machine and its equipment from probable excessive heat. This means that more currents can be drawn from the windings for longer time with the improved cooling system compared to uncooled transformer systems. The metal layer used to allow the heat transmission from the windings to the core and vice versa has a great importance as well since most of the heat is formed in the current-carrying coils.
In the performed successive experimental studies, good results are achieved. With this regard, the proposed study is a powerful alternative to other studies in the literature due to its simplicity and low cost. One should note that better cooling can be achieved with addition of more TEC modules provided that the hot side temperature of the modules can be removed carefully as it can be said that how much better the heat is removed from the hot side, so well done the cooling is.

REFERENCES

Aly, A.A., & El-Lail, A.S.A. (2006). Fuzzy Temperature Control of A Thermoelectric Cooler. IEEE International Conference on Industrial Technolog, Mumbai.

Bulut, H. (2005). Thermoelectric cooling systems. Soğutma Dünyası, 31, 9-16.

Büyükbıçakçı, E. (2006). Cooling Transformators by Using Phase Change Material (PCM). Master thesis, Marmara University, Istanbul.

Carmo, J.P., Antunes, J., Silva, M.F., Ribeiro, J.F., Goncalves, L.M., & Correia, J.H. (2011). Characterization of thermoelectric generators by measuring the load-dependence behavior. Measurement, 44, 2149-2199.

Chein, R., & Chen, Y. (2005). Performances of thermoelectric cooler integrated with microchannel heat sinks. International Journal of Refrigeration, 28, 828-839.

Çiçek, O., Demirel, H., & Tan, S.O. (2001). Design of Blood Transport Container with Thermoelectric Module. Technology, 14, (4), 115-121.

Demirel, H. (2010). Temperature control using peltier devices in hypothermia treatment and its modeling in artificial neural networks. PhD. thesis, Gazi University, Ankara.

Demirel, H., Ciylan, B., Erkal, B., & Yılmaz, S. (2007). Design of a universal thermoelectric module test system for testing rat brain thermoelectric hypothermia. IET Science, Measurement & Technology, 1(3), 160-165.

Dikmen, E. (2002). Determination of factors affecting the operational criteria of thermoelectric coolers and usage area in industry. Master thesis, Süleyman Demirel University, Isparta.

Gürdal, O. (2001). Design of Electrical Machines. Ankara: Atlas+Nobel Publishing. (in Turkish).

Hsu, C.T., Won, C.C., Chu, H.S., & Hwang, J.D. (2013). A Case Study of Thermoelectric Generator Application on Rotary Cement Furnace. International Conference on Microsystems, Packiging, Assembly and Circuits Technology, Taipei.

Ionescu, C., Codreanu, N., & Svasta, P. (2011). Performance Evaluation of a Thermoelectric Cooler Using Finite Element Analysis. 34th International Spring Seminar on Electronics Technology, Tratanska Lomnica.

Kim, S.Y., Lee, K., Park, S., & Kim, J. (2014). Thermal Design Analysis and Performance Test of a 1kW Thermoelectric Battery Cooler. 14th IEEE Intersociety Conference on Thermal and Thermomechenical Phenomena in Electronic Systems, Orlando, FL.

Lineykin S. & Ben-Yaakow, S. (2007). Modeling and Analysis of Thermoelectric Modules. IEEE Transaction on Industry Applications, 43(2), 505-512.

Liu, C.K.., Dai, M.J., Yu, C.K. & Kuo, S.L. (2007). High Efficiency Silicon-based High Power LED Package Integrated with Microthermoelectric Device. Int. Microsystems, Packiging, Assembly and Circuits Tech. Taipei.

Martinez, A., Astrain, D. & Rodriguez, A. (2012) Experimental and analytical study on thermoelectric self-cooling of devices. Energy, 45(1), 874-881.

Shaojing, S., & Qin, Q. (2010). Temperature Control of Thermoelectric Cooler Based on Adaptive NN-PID. International Conference on Electrical and Control Engineering, Wuhan.

Tan, S.O. (2013) Sunucuların Peltier Modüller ile Soğutulması Sisteminin Tasarımı ve Gerçekleştirilmesi. Master thesis, Karabük University, Karabük.

Vinoth, M. & Prema, D. (2014) Automated Car Safety Seat Cooling Systems Using Thermoelectric Cooler. International Conference on Computation of Power, Energy, Information and Communication, Chennai.

Wang, C.C., Hung, C.I., & Chen W.H. (2012). Design of heat sink for improving the performance of thermoelectric generator using two-stage optimization. Energy, 39(1),. 236-245.

Wey, T. (2006). On the Behavioral Modeling of a Thermoelectric Cooler and Mechanical Assembly. IEEE North-East Workshop on Circuits and Systems, Gatineau, Que.

Yalçınkaya, G. (2008). Experimental Power Generation and Cooling with Thermoelectric Module. Master thesis, Dumlupınar University, Kütahya.

Yu, H., Chen, Y., Yu, L., Lu, Y., & Zhang, D. (2012). The Design of Enhancing Thermoelectric Cooler System Based on Forced Air Cooling. International Conference on Systems and Informatics, Yantai.

A BOW-TIE ANTENNA DESIGN FOR BREAST CANCER DETECTION

Emine AVŞAR AYDIN
Adana Science and Technology University
eaydin@adanabtu.edu.tr

Duygu Nazan GENÇOĞLAN
Adana Science and Technology University
dn.gencoglan@ogr.adanabtu.edu.tr

ABSTRACT: Breast cancer is the second in the causes of death ranks after cardiovascular diseases around the world. Early stage cancer detection is the most important in terms of reproducing of the malignant cells in an uncontrolled way and spreading to the other tissues. Microwave imaging is relatively easier compared to other types which are X-ray mammography, Magnetic resonance imaging (MRI) and ultrasound. They have some disadvantages. For example; X-ray mammography suffers from high missed-detection and false-detection rates. Also, it is ionizing and uncomfortable compression of the breast. Because of this, microwave imaging has the potential to overcome the some disadvantages of the X-ray mammography, MRI, and other existing known methods. In addition, Ultra-wide band (UWB) radar technique is a quite attractive technology for many applications, especially for early breast cancer detection. In this paper, both an UWB Bow-tie antenna with enhanced bandwidth and a 3D breast structure which has different permittivity and conductivity is modelled in CST software simulation tool to solve electromagnetic field values. Besides, The Federal Communications Commission (FCC) allowed frequency bandwidth of 3.1 to 10.6 GHz for this aim. Return loss, VSWR, and radiation pattern characteristics which are significant antenna parameters are simulated and obtained whether the antenna possess an efficient characteristic or not. Also, electric field values over the breast tissue with tumor and without tumor are evaluated.

Key words: Bow-tie antenna, breast cancer, microwave imaging, CST

INTRODUCTION

When uncontrolled growth (division beyond the normal limits) is occurred in a group of cells, this disease is called as cancer, invasion (intrusion on and destruction of adjacent tissues), and sometimes metastasis (spread to other locations in the body via lymph or blood) [1, 2]. Cancer cells which spread into different tissues cause various diseases; namely breast cancer, skin cancer, lung cancer, kidney cancer, prostate cancer, thyroid cancer etc. Breast cancer, which is a vital cause of death among women, is increasingly becoming a crucial interest

around the world. Additionally, breast cancer usually occurs either in the cells of the lobules, or the ducts. However, every woman has her menstrual cycle due to the nature. In these cycles, breasts of women have different structures. At the same time, the structure of the breast tissue shows differences with age. For instance, breast tissue of young women has glands and milk ducts, but breast tissue of old women has mostly fatty tissue. There are also some external effects which causes breast cancer such as life-style, foods, contamination, stress, drugs, cigarette, alcohol and its derivatives etc. Therefore, early breast cancer detection is a big challenge task for the researchers and healthcare professionals in order to prevent the metastasis.

Hitherto; there have been a great many tools for early detections including mammogram, X-ray mammography, magnetic resonance imaging (MRI), ultrasound, electrical impedance tomography (EIT) etc.[3, 4] . X-ray mammography is one of the most widely-used detection technique [1, 5]. However the X-ray contrast between a tumor and the surrounding tissue is of the order of a few percent and as a result it suffers from relatively high missed-detection and false-detection rates. X-rays are also ionizing and not generally used to frequent screening. At the same time, X-ray mammography is uncomfortable compression of the breast. EIT which is one of the detection techniques has interested as a low-cost, non-invasive imaging tool for human body[6]. It is known that cancerous tissue has a much higher conductivity and permittivity than normal tissue. So, EIT may also be useful in the detection of breast cancer. These electrical properties (conductivity and permittivity) are changed very early in the cancerous cycle. Because of this, EIT may be used to detect cancer or tumor. However EIT would be acceptable on younger women. Conversely, these methods are not sufficient because of limitations. Recently, a novel method is Active Microwave Imaging (AMI) including Microwave Tomography and Ultra-Wideband (UWB) Radar based approach due to low cost and non-ionizing feature [1, 7, 8] . UWB radar based approach systems have attractive research area. Antenna structure is a key component in UWB applications. UWB antenna is also applied to define tumor in UWB Radar based approaches.

The key problem with the antenna design procedure is that the proposed antenna bandwidth should comply with the UWB requirements [9]. As a drawback from the previous chapter (Half wave dipole), bandwidth of half wavelength dipole is narrow. Thus, quite a few design techniques might be used to increase the bandwidth. One of the techniques for the half wavelength dipole antenna is to modify the structure of the dipole. A considerable amount of antenna shape has been designed and investigated in the literature [10-14]. The different antenna configurations, especially dipole configurations, are taken into account for the UWB requirements i.e circular, square, triangular, other shapes which have two metal sheets such as bow tie. Modified dipole configurations are generally preferred to get the broadband characteristic. The main point is that the antenna features should be light weight, low cost, ease of fabrication during the

modification process. As mentioned before, the bow tie antenna is definitely one of the dipole configurations. Bow tie antenna has wider bandwidth than half wave dipole despite the simplicity structure.
In this paper, bow-tie antenna is designed for the purpose of microwave imaging over detecting cancerous tissue into breast structure and also, a simple 3D breast structure is modelled to define cancerous tissue. Different simulations such as breast tissue with tumor and without tumor are implemented in CST Microwave Studio. Obtained simulation graphics are evaluated according to electric field values.

BREAST STRUCTURE

By using the CST Software, data for the UWB microwave imaging techniques are obtained from numerical breast phantoms [2, 3]. There have been several breast phantom models in the literature, including cylindrical, hemispherical, and MRI-derived models. In this paper, a hemispherical breast is modelled as shown in Figure 1. Diameters and thicknesses of breast model are shown in Table 1. Also, the tumor radius size ranges from 0.2 cm to about 1.5 cm. Tumor is modelled as a spherical structure and is placed in the breast tissue (fibro glandular tissue). Structures such as skin, fatty breast tissue, tumor have different dielectric properties (permittivity, conductivity) have different electromagnetic field values. Differences of dielectric properties provide opportunity for detecting of tumor. The dielectric properties are given in Table 2 [15].

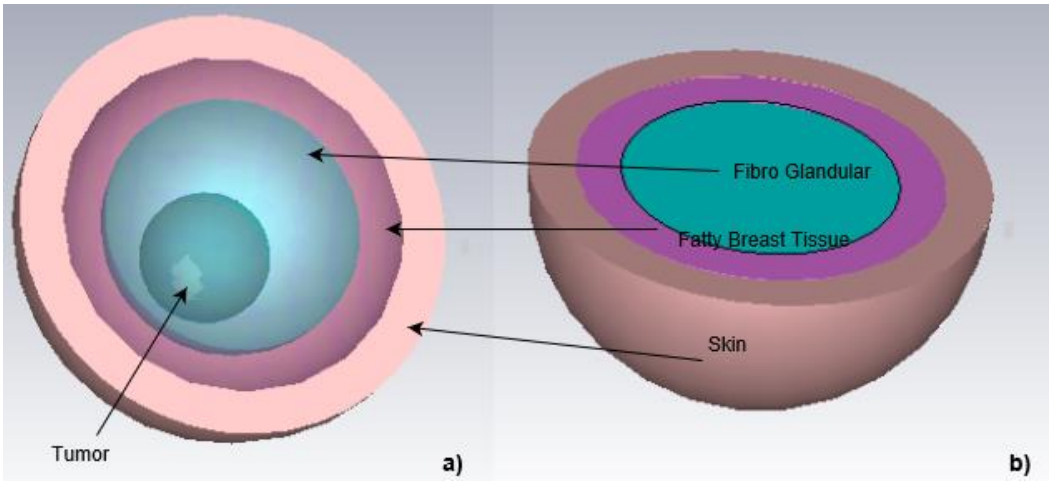

Figure 1. 3D Breast Structure, a) top view b) side view

Table 1. Dimensions of parts of the breast

Model Part	Diameter	Thickness
Skin	10mm	2mm
Fatty Breast	8mm	2mm
Fibro Glandular	6mm	2mm

Table 2. Debye parameters at 6 GHz UWB Centre Frequency [15]

Tissue	ε_∞	ε_s	σ_s	τ(ps)
Skin	4.00	37.00	1.10	7.37
Fatty breast tissue	6.57	16.29	0.23	7.00
Fibro glandular	5.28	35.14	0.46	7.0
Tumor	3.99	54.00	0.70	7.23

ANTENNA STRUCTURE

Arrangement and dimensions of the bow tie antenna is depicted in Figure 2.The proposed antenna is printed on substrate with dielectric constant of 2. The thickness of the substrate is 0.5 mm. The all length of proposed antenna must be slightly equal to $\lambda/2$ for perfectly radiation efficiency .The antenna is composed of two dielectric metal sheets that have 55 mm length per sheet. The bowtie antenna is represented by two metal sheets which have lengths l_e (55 mm) and separated by feeding gap (0.66 mm).Flare angle (α) is 60^o which is determined the distance between two metal sheets. Any changes in antenna size affect the performance of antenna parameters. Therefore, any antenna size should be fixed by varying another antenna size in order to obtain bandwidth enhancement. The design parameters such as arm length, substrate width, feed gap, permittivity and flare angle are optimized to obtain the better bandwidth and gain characteristics by antenna designers as in [13]. Substituting the value of the lower frequency and the upper frequency into Equation (1), the center frequency is computed. The bowtie antenna presented this section has been designed using dimensions in Figure 2. CST Microwave Studio is used to simulate this bow tie model with bow-tie antenna and breast structure as shown in Figure 3.

$$f_{center} = \frac{f_{upper} + f_{lower}}{2} \quad (1)$$

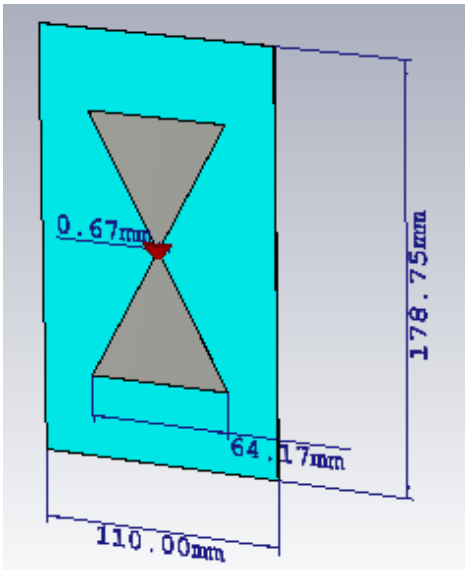

Figure 2. Proposed Antenna Structure (Bow-Tie Antenna)

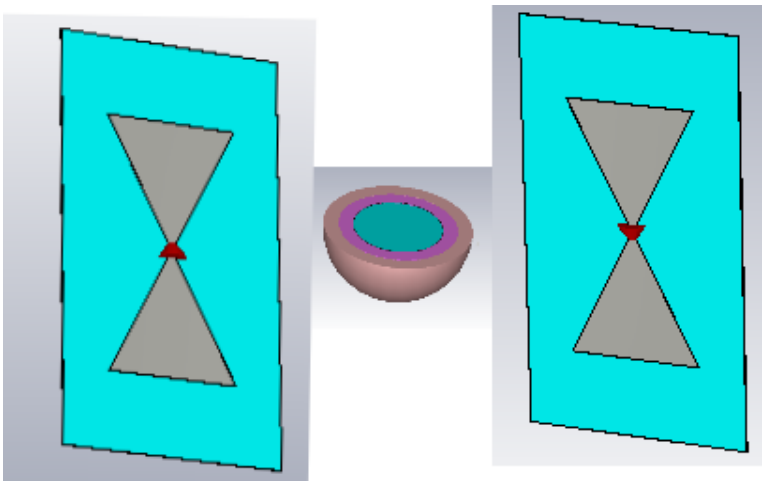

Figure 3. Design with proposed antenna and breast structure

SIMULATION RESULTS

Analysis of proposed antennas are carried out and presented. Parameters which are analyzed are return loss, radiation pattern and VSWR. The proposed antenna's -10 dB bandwidth which spans in 3.1-10.6 GHz is achieved as given in Figure 4. These frequency range meets the requirements for UWB imaging systems which is especially used for early breast cancer detection. Additionally, VSWR of the proposed antenna illustrates in Figure 5. VSWR has also desired characteristic in the frequency of interest.

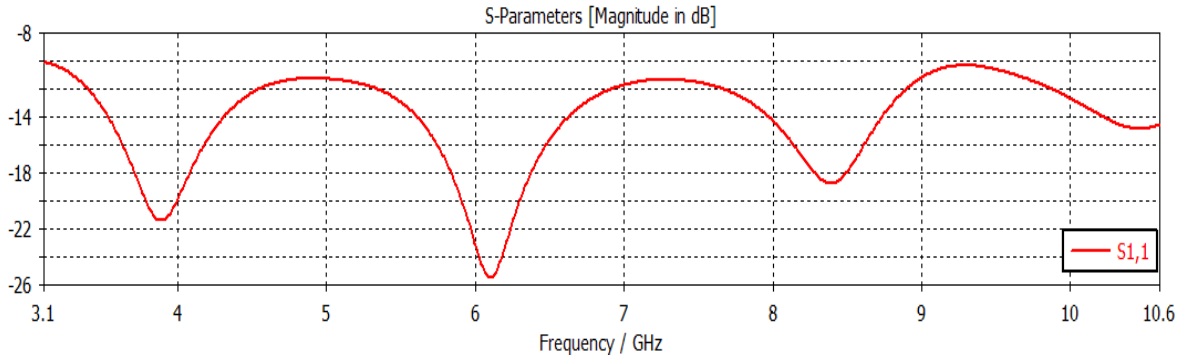

Figure 4. Graphic of S-parameter (S_{11}) of designed Bow-tie antenna

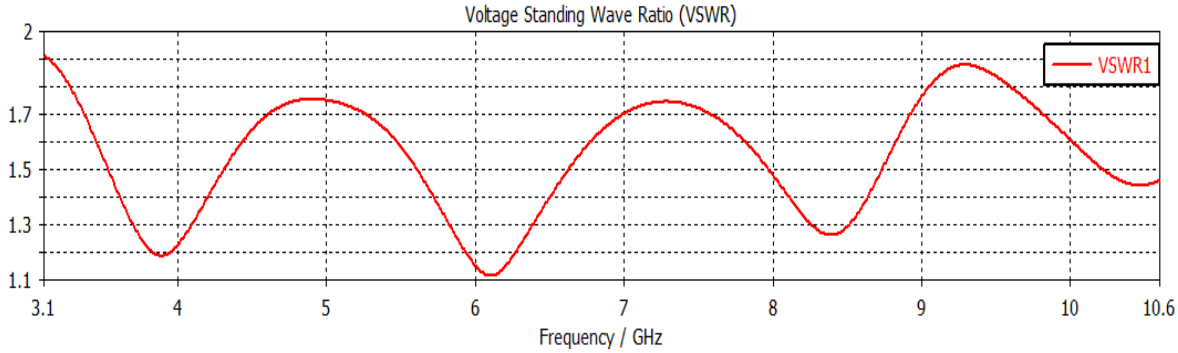

Figure 5. Graphic of Voltage Standing Wave Ratio of designed Bow-tie antenna

Figure 6 illustrates the radiation pattern characteristic of the proposed antenna at four different frequencies 3, 4.5, 7.5, 9 GHz respectively. Four of them has omnidirectional radiation pattern characteristics which is acceptable feature for a better coverage of the breast surface.

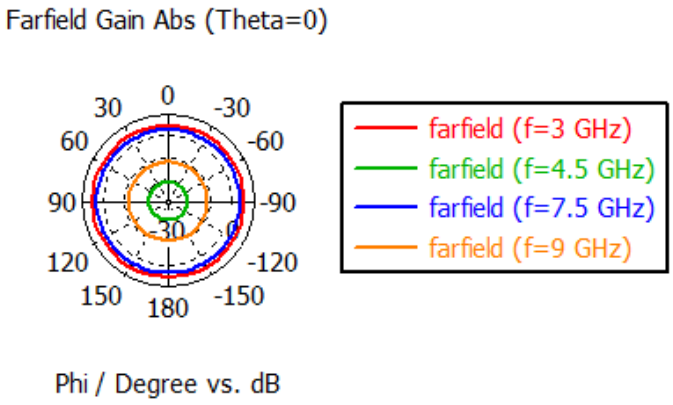

Figure 6. Radiation pattern of designed Bow-tie antenna at different frequencies 3, 4.5, 7.5, 9 GHz respectively

The breast structure is simulated with an excitation signal from the bowtie antenna and the electric fields values are obtained for different tumor size such as 2, 3, 4 mm respectively in order to detect the cancerous cells. Additionally, it is

observed that both breast tissues with tumor and without tumor have significantly difference in the electric field. Figure 7 illustrates the maximum electric field value of the breast tissue without tumor at given position (0, 5, 10. 95). Figure 8,9,10 show the maximum electric field value of the breast structure with different tumor sizes. Furthermore, Table 3 shows electric field values for breast tissue with different radius tumors and without tumor. Differences between values of breast structure with tumor and without tumor are clearly shown in Table 3.After all, tumor in the breast structure can be detected due to the electric field difference.

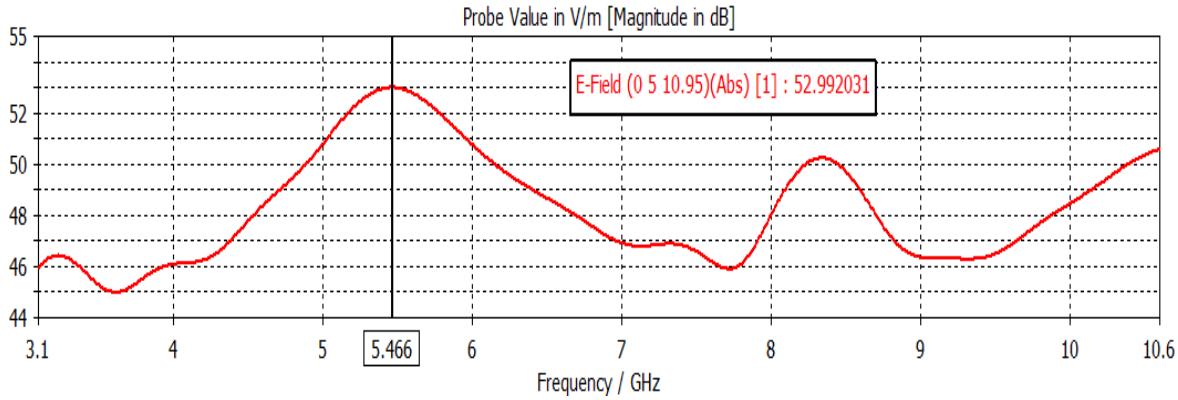

Figure 7. Graphic of electric field of breast tissue without tumor

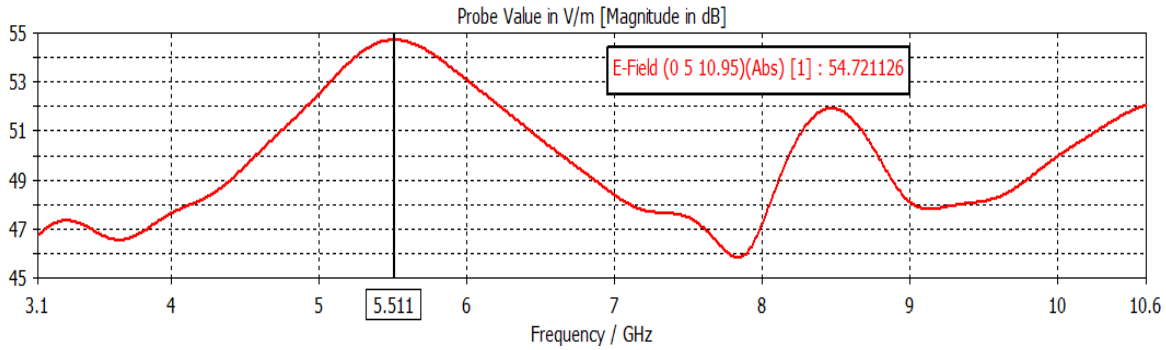

Figure 8. Graphic of electric field of breast tissue with tumor (tumor radius is 2mm)

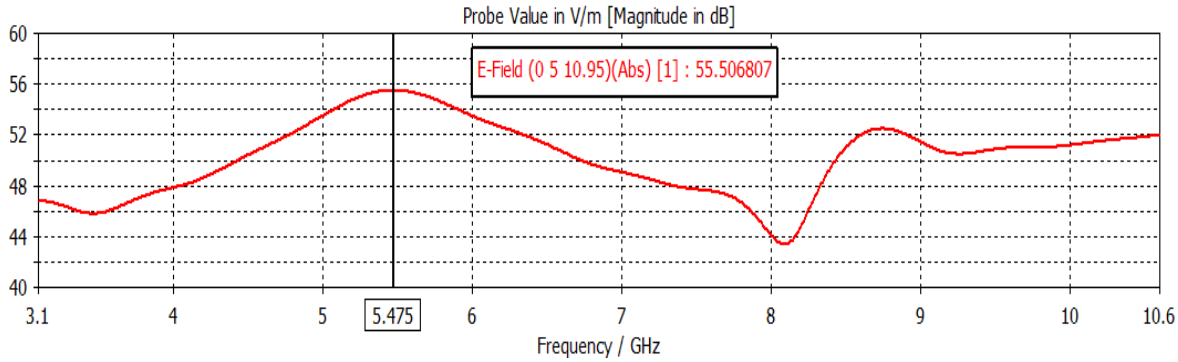

Figure 9. Graphic of electric field of breast tissue with tumor (tumor radius is 3mm)

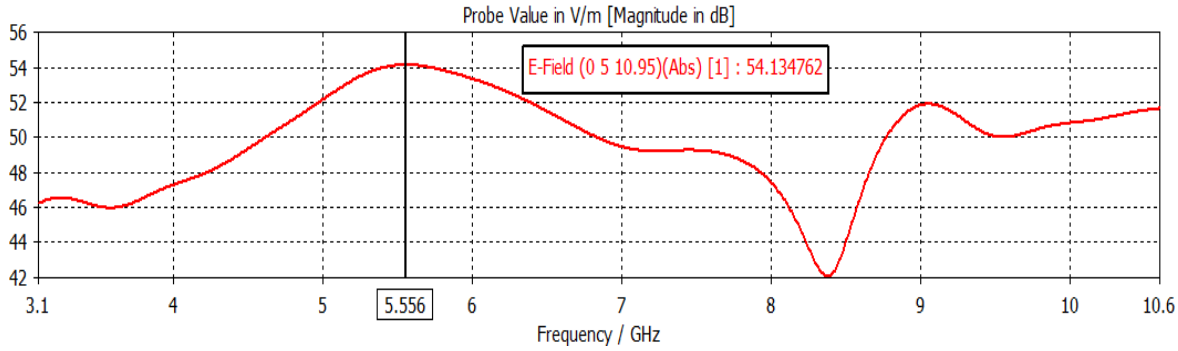

Figure 10. Graphic of electric field of breast tissue with tumor (tumor radius is 4mm)

Table 3. Obtained electric field values according to breast tissue with tumor and without tumor

Tumor Radius	E_{max}(with tumor)	E_{max} (without tumor)
2 mm	54.72 V/m	52.99 V/m
3 mm	55.51 V/m	52.99 V/m
4 mm	54.14 V/m	52.99 V/m

CONCLUSION

In this paper, a bow-tie antenna is used to diagnose tumor due to its low profile, high bandwidth and omnidirectional radiation pattern. Firstly, a bow-tie antenna is designed in order to cover UWB frequency range (3.1-10.6 GHz). Secondly, a 3D breast structure which is made up of skin layer, fatty layer and fibro glandular layer is obtained. Then, this antenna structure and breast structure are simulated in CST software simulation tool to diagnose the tumor cells. Finally, the electric fields values are measured with different tumor size. All these values are acceptable for detecting breast tumor.

REFERENCES

1. Munawar, A., et al. Breast cancer detection using Forward Scattering Radar technique. in RF and Microwave Conference, 2008. RFM 2008. IEEE International. 2008.

2. Chouiti, S.M., et al., An Efficient Image Reconstruction Method for Breast Cancer Detection Using an Ultra-Wideband Microwave Imaging System. Electromagnetics, 2016. 36(4): p. 225-235.

3. Çalışkan, R., et al., A Microstrip Patch Antenna Design for Breast Cancer Detection. Procedia-Social and Behavioral Sciences, 2015. 195: p. 2905-2911.

4. Afyf, A., et al., A Novel Low Cost UWB Antenna for Early Breast Cancer Detection. American Journal of Electromagnetics and Applications, 2015. 3(5): p. 31-37.

5. Nilavalan, R., et al., Wideband microstrip patch antenna design for breast cancer tumour detection. IET Microwaves, Antennas & Propagation, 2007. 1(2): p. 277-281.

6. Kejariwal, M., et al. Breast cancer detection using electrical impedance tomography: spice simulation. in Engineering in Medicine and Biology Society, 1993. Proceedings of the 15th Annual International Conference of the IEEE. 1993. IEEE.

7. Yun, X., E.C. Fear, and R.H. Johnston, Compact antenna for radar-based breast cancer detection. IEEE Transactions on Antennas and Propagation, 2005. 53(8): p. 2374-2380.

8. Klemm, M., et al., Radar-based breast cancer detection using a hemispherical antenna array—experimental results. IEEE Transactions on Antennas and Propagation, 2009. 57(6): p. 1692-1704.

9. Commission, F.C., Revision of part 15 of the commission's rules regarding ultrawideband transmission system. 2002.

10. Sayidmarie, K.H. and Y.A. Fadhel, A planar self-complementary bow-tie antenna for UWB applications. Progress In Electromagnetics Research C, 2013. 35: p. 253-267.

11. Dona Mary George, R.R., Design and Analysis of Different Bow-Tie Configurations for Submarines. IJRCCE, 2015. 3(9).

12. Zhang, X., et al. Integrated broadband bowtie antenna on transparent substrate. in SPIE OPTO. 2015. International Society for Optics and Photonics.

13. Çolak, Ş. and D.N. Gençoğlan. Improvement of bowtie antenna parameters for Ultra-Wide Band applications. in 2016 24th Signal Processing and Communication Application Conference (SIU). 2016. IEEE.

14. Sharma, C., S.B. Rana, and H. Singh, Design and Analysis of Modified Bowtie Antenna. International Journal of Technology Enhancements and Emerging Engineering Research 2015. 3(05): p. 119-121.

15. Ikram, E., et al., Improved debye model for experimental approximation of human breast tissue properties at 6 GHz ultra-wideband centre frequency. 2013.

IMPROVEMENT OF MAGNETIC PROPERTIES OF MELT-SPUN PRODUCED $Nd_2Fe_{14}B$ PARTICLES DURING SURFACTANT-ASSISTED BALL MILLING

Sultan ÖZTÜRK[1]
[1]Karadeniz Technical University, Faculty of Engineering, Department of Metallurgical and Materials Engineering, 61080, Trabzon, TURKEY
suozturk@gmail.com

Kürşat İCİN[1]
kursaticin@ktu.edu.tr

Bülent ÖZTÜRK[1]
bozturk@ktu.edu.tr

Uğur TOPAL[2]
TUBİTAK National Metrology Institute, 5441470, Kocaeli, TURKEY
ugur.topal@tubitak.gov.tr

Hülya KAFTELEN[1]
hkaftelen@ktu.edu.tr

ABSTRACT: NdFeB permanent magnets are used for variety of applications such as electronics, automotive and clean technology industries. The majority of commercial NdFeB permanent magnets are produced by melt-spinning techniques and sintering. The sintered NdFeB magnets represent about 90% of the total rare earth permanent magnet market. Sintered melt-spin NdFeB magnets exhibit the highest magnetic performance due to their strong crystallographic alignment. These magnets have enabled their applications to operate with the highest energy efficiencies and to be fabricated in the most compact form. In this study, the flaky shaped $Nd_{15}Fe_{77}B_8$ magnetic alloy powders were produced by melt-spinning technique. In this process, the powders were produced by using a single roller melt spinning apparatus with high vacuum atmosphere (10^{-7} mbar). The flaky shaped $Nd_{15}Fe_{77}B_6$ powders were milled by using the high energy ball milling under vacuum atmosphere with surfactant-assisted material. The experiments were performed to optimize the milling parameters regarding the particle size and magnetic properties of the powders.

Key words: $Nd_{15}Fe_{77}B_8$ magnetic alloy, Melt spinning, Surfactant-assisted)

INTRODUCTION

The NdFeB magnets with excellent properties have extended the applications in the field of motors such as hybrid electric vehicles and electric vehicles. In recent years, there is a trend of permanent magnet motors replacing traditional motors, because they have high efficiency and can run on lower energy. Therefore, the sintered NdFeB magnets with high coercivity have much appeal for the scientist and engineers (Yan et al., 2011). There are two major commercialized process routes for the production of NdFeB permanent magnets. The first method is powder metallurgy and the second one is the melt spinning process. The majority of commercial NdFeB permanent magnets are produced by powder metallurgy and melt-spinning techniques. In recent years, the melt spinning technique has attracted rapidly increasing interest in NdFeB alloys because it can be used to produce reliable materials for bonded magnets or to directly produce thin plate-shaped, permanent magnets for diverse applications (Tian et al., 2004). This process is used to make rapidly solidified microcrystalline and amorphous alloy ribbon, flake, etc. Moreover, it is possible to obtain a supersaturated solid solution with a higher quantity of alloying elements, and to avoid or minimize the formation of second phases. Sintered melt-spin NdFeB magnets exhibit the highest magnetic performance due to their strong crystallographic alignment. These magnets have enabled their applications to operate with the highest energy efficiencies and to be fabricated in the most compact form (Brown, Wu, He, Miller, & Herchenroeder, 2014). There are many factors that govern the suitability of a permanent magnets such as coercivity, high remanence (B_r) and maximum energy product ($(BH)_{max.}$). These hard magnetic properties strongly depend on the mean particle size of the NdFeB powders. This dependence is a result of interactions: smaller the mean powder size, higher the coercivity (Szymura, Wyslicki, Rabinovich, & Bala, 1994). High energy ball-milling is a simple, inexpensive and efficient technique for the size reduction of micro or nanocrystalline powders (Neu & Schultz, 2001; Ono et al., 2002). The main advantage of the ball milling method is the applicability of this method to large scale production. and high purity of the powders. On the other hand, this method hosts some deficiencies in term of the purity of the powders. In this sense, the oxidation of the milled powders is main concern because it affects the subsequent process steps such as pressing, sintering and the magnetic properties of resultant product (Chandrasekaran, 2007). For this reason, it is essential to use protective agents during high energy ball milling process to avoid the oxidation of the powders. It has been reported that the rare-earth intermetallic compounds powders were ball milled in the presence of an organic liquid and surfactants, and this method is called as surfactant assisted ball milling (SABM) (Simeonidis et al., 2011). This technique has become a novel approach for the preparation of NdFeB particles and flakes (Su et al., 2013). Surfactants help to decrease the particle size and facilitate shape homogeneity during the milling process. Surfactant agents have also important chemical protection and lubrication to the powder surfaces. In this regard, the surfactant helps to decrease local heating, contamination and oxidation of the powders (Simeonidis et al., 2011).

In the present study, we have investigated the changes in size, morphology, thermal and magnetic properties of magnetically hard $Nd_{15}Fe_{77}B_8$ alloy powders by using a surfactant assistant high energy ball milling method.

METHODS

Commercial magnetic alloy ingot with nominal composition of $Nd_{15}Fe_{77}B_8$ (at %) was used to produce flaky shaped powders. The rapidly solidified $Nd_{15}Fe_{77}B_8$ alloy powders have been produced by using a laboratory scale single roller melt spinning device operating in high vacuum atmosphere (10^{-7} mbar). Small amounts of the crushed ingots were placed in a hexagonal boron nitrite crucible with slit shape nozzle of 10x0,7 mm at the bottom. The ingots were induction melted and superheated to about 1350 °C in a vacuum atmosphere. The temperature of the melt was monitored by infrared thermometer. The molten alloy was ejected through slit shape nozzle with compressed argon gas of 0,25 bar onto rotating cooper wheel (27 cm diameter) at a surface velocity of 52 m/s (maximum speed of wheel) under vacuum atmosphere. Milling process of the rapidly solidified flaky shaped powders by melt spinning method was performed in an atmosphere of oxygen free inert environment (vacuum atmosphere, 10^{-3} mbar) with addition of protective surface active agents. The oleic acid (99,9 purity) was used as surfactant and heptane and hexane (99,9 purity) were added as an organic solvent during milling process. Fritsch Pulverisette 6 type high energy ball miller was used and the flaky shaped powders were ground in a 250 ml capacity milling jar made of tool steel and boron-carbide surface hardened. 5 mm diameter tungsten carbide balls were used and the rotational speed of the jar was kept constant as 300 rpm. The weight ratio of the balls to the powders ($\mu = m_{ball}/m_{powders}$) was 10:1. The amounts of surfactant and organic solvent used were about 10 – 12% by weight of the starting powders and milling times were varied from 1,5 to 6,5 hours. After the milling process, the slurry mixture of powders and surfactant material were obtained. Cleaned powders were achieved with the processes of washing with ethanol and centrifugal drying.

The phase structured of the sample was examined by x-ray diffraction (XRD) at room temperature using PANalytical X'pert^3 Powder diffractometer with Cu Kα radiation. Scanning electron microscopy (SEM) was employed to examine the morphology, mean particle size and microstructure of the particles. The magnetic properties of particles were measured by Physical Properties Measurements System (PPMS) equipment with 9 T vibrating sample magnetometer (VSM).

RESULTS AND FINDINGS

The melt spinning is a method of producing rapidly solidified ribbons. However, Nd-Fe-B alloy powders, instead of ribbon were produced by melt spinning method because brittle character of the $Nd_{15}Fe_{77}B_8$ alloy, in this study. Morphology of produced $Nd_{15}Fe_{77}B_8$ magnetic alloy powders by melt spinning method is seen

in Fig. 1.a. As can be seen from the figure, the shape of the produced powders is characterized by irregular and flake form (Yan et al., 2011). The flaky shaped powders have 25-100 µm width and 80-600 µm length. The thickness of these particles varied between 5-48 µm. The microstructure of the $Nd_{15}Fe_{77}B_8$ alloy powders produced by the melt spinning method was given in Fig.1.b. Predominant shape of the microstructure was equiaxed cellular and the mean cell size was decreased with decreasing powder size and decreasing the thickness of the flaky shaped powders. The mean cell sizes for 5 and 48 µm powders were measured as 0.69 µm and 1.3 µm, respectively. There is a direct relationship between microstructural grain size and cooling rate for the produced powders. The cooling rate increases with decreasing cell size.

For calculation of the cooling rate of the powders, the equation given in (Ozawa, Saito, & Motegi, 2004) was used. The cooling rates of 5 and 48 µm thick flaky shaped powders were calculated as $4.3x10^{-6}$ K/s and $4.7x10^{-5}$ K/s, respectively. Besides microstructural examinations of produced powders, EDX analysis was also made to reveal the phase structures of the powders. Fig. 1.b shows the back-scattered microstructure of produced powder. As can be seen from Fig.2, the micrograph exhibits the dark equiaxed grain matrix together with the white grain boundary. The present of phases was identified by virtue of EDX analysis According to the EDX analysis, the matrix consists of $Nd_2Fe_{14}B$ hard magnetic phase located in grain interior and the grain boundary is the Nd-rich phase which is soft magnetic properties. From the EDX analysis the elementel composition of grain interior by wt. percentage are 27.58% Nd, 62.44% Fe and 9.98% B. These values indicate the nominal composition of magnetically hard $Nd_2Fe_{14}B$ phase.

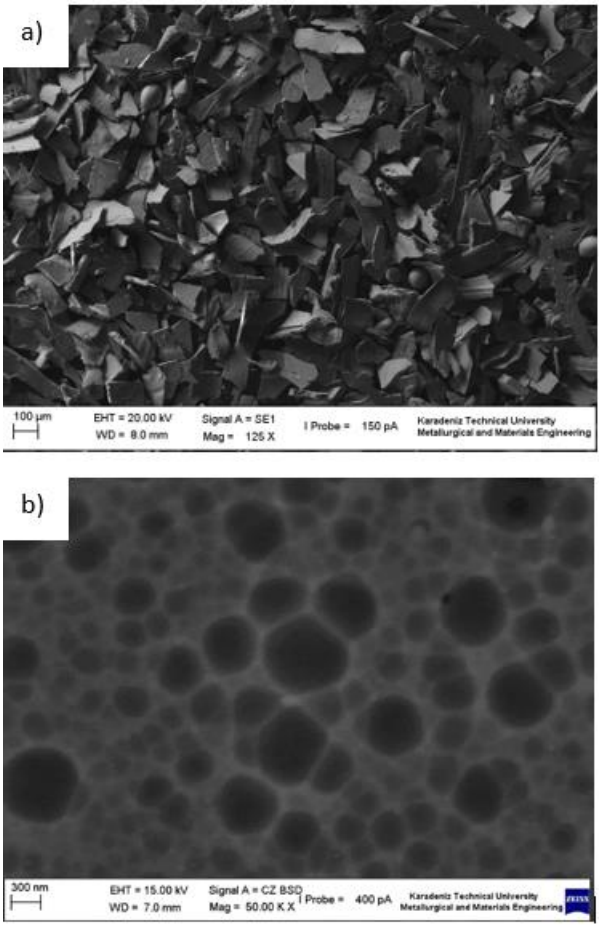

Figure 1. a) rapidly solidified of NdFeB powders by melt spinning method, b) Microstructure of $Nd_{15}Fe_{77}B_8$ magnetic alloy ribbons.

The XRD pattern of the unmilled flake powders are presented in Figure 2. As can be seen, produced flaky powders mainly consists of $Nd_2Fe_{14}B$ hard magnetic phase. Besides this phase, magnetically soft α-Fe (primer iron) and Nd-rich phases were observed in small quantity in the melt spun powders. The α-Fe phase is often found in Nd-Fe-B system alloys, because the $Nd_2Fe_{14}B$ phase is formed by peritectic reaction of liquid and the primary α-Fe phase.

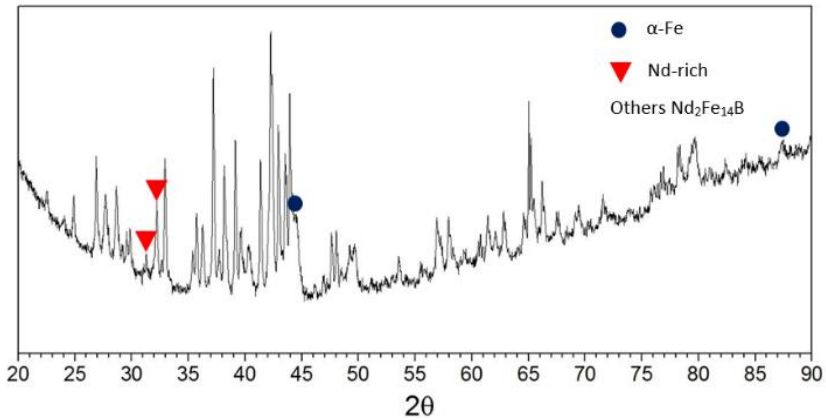

Figure 2. Diffraction pattern of $Nd_{15}Fe_{77}B_8$ magnetic flake powder.

Figure 3. shows the SEM micrographs of the high energy ball milled $Nd_2Fe_{14}B$ particles obtained with various milling times. As stated above, only milling time was changed while other parameters were kept constant. The powders were milled for six different milling times of 90, 150, 210, 270, 330, 390 min in the oleic acid environment. As can be seen from the figure, the particles agglomerated with increasing milling time and decreasing particle size. In the high energy ball milling, the large particles break as a result of the internal strain created by the high pressure exerted on the particles. On the other hand, the finely divided particles tend to agglomerate in order to minimize their surface energy. But, the presence of solvent and surfactant in SABM is known to be very efficient at preventing cold welding and the agglomeration of particles during ball milling. Surfactant covering a particle or flake can lower the surface, enabling long-range capability forces and lowering the energy required for crack propagation (Lewis, Panchanathan, & Wang, 1997).

The internal strain in the particles increases rapidly at the beginning of the ball milling, so large sized micro or nanocrystalline powders produced by melt spinning method break into tens of micrometers or micro sized irregular particles. Then, micro cracks start from an easy cleavage plane in the particles and the grain. At the edge of the grain, the development of micro crack is prevented due to crystal mismatch between grains. The micro crack could spread through the grain boundary into the adjacent grains until the internal strain concertation is sufficiently high (Su et al., 2013).
The variation of mean particle size with milling time was given in Fig. 4. As can be seen, the mean particle size decreased with increasing milling time. The mean particle sizes obtained are 1.481, 1.214, 0.948, 0.872, 0.431 and 0.266 μm for 90, 150, 210, 270, 330, 390 min. milling times, respectively.

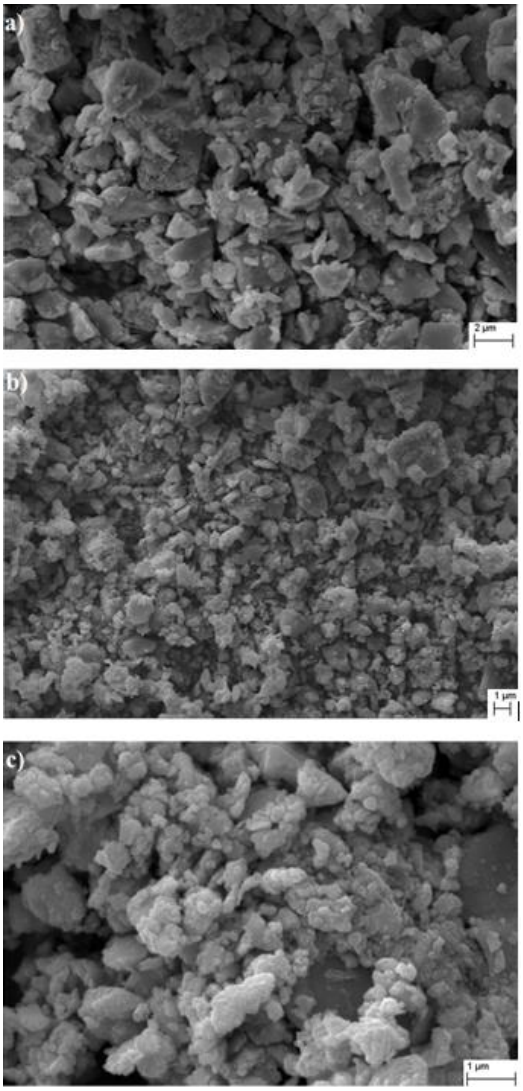

Figure 3. SEM images of NdFeB powders obtained by ball milling with various milling times: a) 90 min., b) 210 min. and c) 390 min

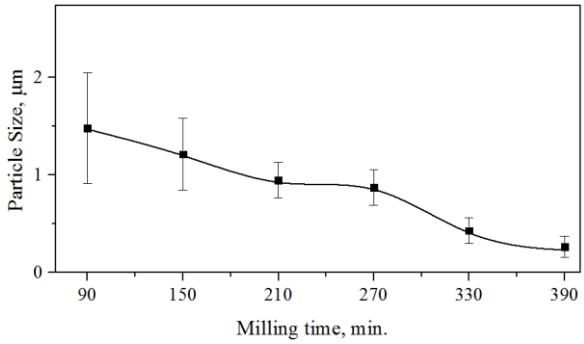

Figure 4. Effect of ball milling time on the mean particle size of the NdFeB powders.

Magnetic hysteresis loops were recorded for the starting powder and different milling times in Figure 6. The coercivity of the Nd-Fe-B alloys is not only heavily dependent on the grain size of the $Nd_2Fe_{14}B$ phase but also on the amounts of the soft magnetic phases such as α-Fe phase and Nd-rich phase. The appearance of irregularities in the hysteresis of the unmilled flake powders by melt spinning

process is attributed to the presence of the soft magnetic phases of Nd-rich and α-Fe.

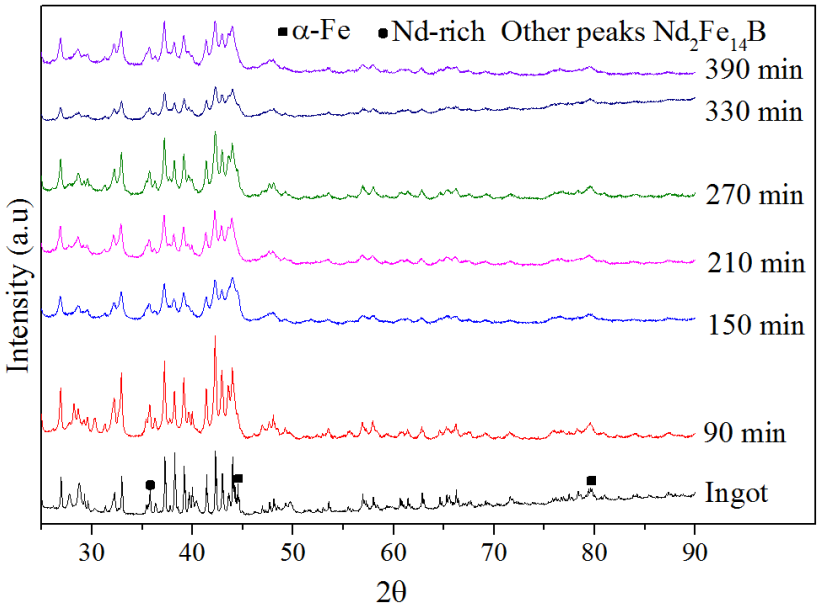

Figure 5. XRD pattern of the starting ingot magnetic alloy and milled powder with various times.

Figure 7. illustrates the variation of coercivity with milling time from 90 to 390 minutes. The figure shows the coercivity increase with increasing milling time. The maximum coercivity (4.250 kOe) is attained after 330 minutes. Further increase of SABM time leads to the decrease of coercivity following the evolution of particle isolation and the dimension reduction. According to literature, at high milling periods, the magnetic anisotropy of the powder is reduced by the time. However, the presence of the elongated particles shape anisotropy (Rong, Poudyal, & Liu, 2010; Simeonidis et al., 2011)

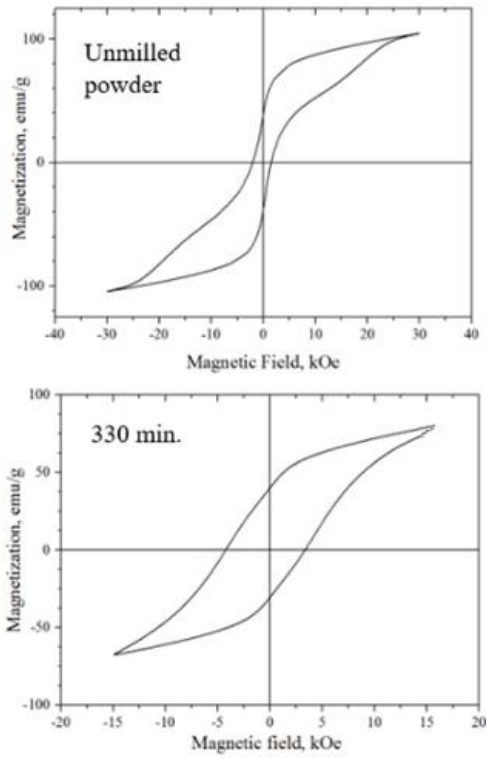

Figure 6. Hysteresis loops of the unmilled flake powders and after SABM for 330 minutes.

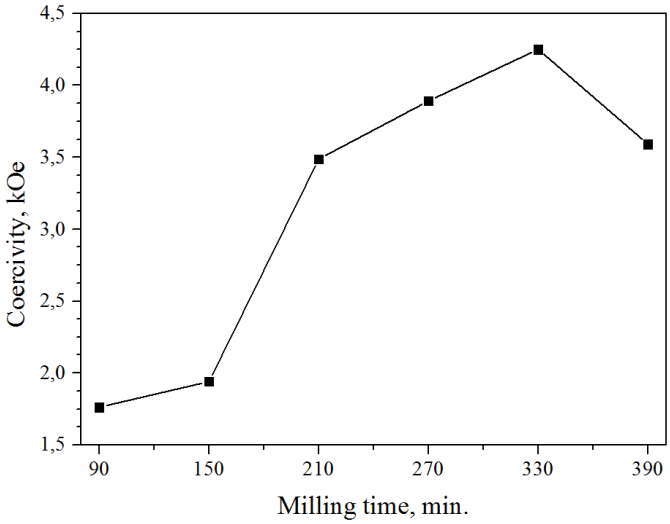

Figure 7. Coercivity of powder as a function of the different SABM times.

CONCLUSIONS

1. The mean cell sizes of produced flaky shaped powders by melt spinning method were increased with decreasing cooling rate.
2. The mean particle size of milled powders decreased with increasing milling time.

3. According to XRD analysis, the diffraction peaks of the $Nd_2Fe_{14}B$ hard magnetic phase are observed in all samples produced with SABM. Besides that, soft magnetic phases of Nd-rich and α-Fe are observed in samples.
4. The coercivity of milled powders increase with increasing milling time. The maximum coercivity is attained after 330 minutes. increase of SABM time leads to the decrease of coercivity following the evolution of particle isolation and the dimension reduction.

ACKNOWLEDGMENTS

This work is supported by the scientific and technological research council of Turkey (TUBİTAK) with project number 114M501. The authors would like to thanks TUBİTAK for the support.

REFERENCES

Brown, D. N., Wu, Z., He, F., Miller, D. J., & Herchenroeder, J. W. (2014). Dysprosium-free melt-spun permanent magnets. Journal of Physics: Condensed Matter, 26(6), 64202. http://doi.org/10.1088/0953-8984/26/6/064202

Chandrasekaran, P. S. and R. G. and N. V. R. R. and M. M. R. and V. (2007). SmCo 5 /Fe nanocomposite magnetic powders processed by magnetic field-assisted ball milling with and without surfactant. Journal of Physics D: Applied Physics, 40(17), 5021. http://doi.org/10.1088/0022-3727/40/17/002

Lewis, L. H., Panchanathan, V., & Wang, J. Y. (1997). Technical magnetic properties of melt-spun (Nd1-xPrx)(2)Fe14B at low temperature. Journal of Magnetism and Magnetic Materials, 176(2–3), 288–296. http://doi.org/10.1016/S0304-8853(97)00648-3

Neu, V., & Schultz, L. (2001). Two-phase high-performance Nd-Fe-B powders prepared by mechanical milling. Journal of Applied Physics, 90(3), 1540–1544. http://doi.org/10.1063/1.1380223

Ono, K., Kakefuda, Y., Okuda, R., Ishii, Y., Kamimura, S., Kitamura, a., & Oshima, M. (2002). Organometallic synthesis and magnetic properties of ferromagnetic Sm-Co nanoclusters. Journal of Applied Physics, 91(10 I), 8480–8482. http://doi.org/10.1063/1.1456407

Ozawa, S., Saito, T., & Motegi, T. (2004). Effects of cooling rate on microstructures and magnetic properties of Nd-Fe-B alloys. Journal of Alloys and Compounds, 363(1–2), 263–270. http://doi.org/10.1016/S0925-8388(03)00461-4

Rong, C., Poudyal, N., & Liu, J. P. (2010). Size-dependent spin-reorientation transition in Nd2Fe14B nanoparticles. Physics Letters A, 374(38), 3967–3970. http://doi.org/10.1016/j.physleta.2010.07.061

Simeonidis, K., Sarafidis, C., Papastergiadis, E., Angelakeris, M., Tsiaoussis, I., & Kalogirou, O. (2011). Evolution of Nd2Fe14B nanoparticles magnetism during surfactant-assisted ball-milling. Intermetallics, 19(4), 589–595. http://doi.org/10.1016/j.intermet.2010.12.012

Su, K. P., Liu, Z. W., Zeng, D. C., Huo, D. X., Li, L. W., & Zhang, G. Q. (2013). Structure and size-dependent properties of NdFeB nanoparticles and textured nano-flakes prepared from nanocrystalline ribbons. Journal of Physics D: Applied Physics, 46(24), 245003. http://doi.org/10.1088/0022-3727/46/24/245003

Szymura, S., Wyslicki, J., Rabinovich, Y., & Bala, H. (1994). Domain structure, magnetic and mechanical properties of Nd-Fe-B magnets with different grain size. Phys. Stat. Sol. (a), 141, 435.

Tian, Z., Li, S., Peng, K., Gu, B., Zhang, J., Lu, M., & Du, Y. (2004). The microstructure and magnetic properties of NdFeB magnets directly solidified at a low cooling rate. Materials Science and Engineering A, 380(1), 143–146. http://doi.org/10.1016/j.msea.2004.03.077

Yan, G. H., Chen, R. J., Ding, Y., Guo, S., Lee, D., & Yan, a R. (2011). The preparation of sintered NdFeB magnet with high-coercivity and high temperature-stability. Journal of Physics: Conference Series, 266(1), 12052. http://doi.org/10.1088/1742-6596/266/1/012052

SOIL EROSION RISK IN BARAK PLAIN FROM THE PERSPECTIVE OF THE ENVIRONMENTALISTS

Erdihan Tunç*, Şahabettin Doğan

University of Gaziantep, Faculty of Arts & Science, Department of Biology, 27310 Şehitkamil, Gaziantep, Turkey

*Corresponding author: Tel.: +(90342-3171948) Fax: +(903423601032), tunc@gantep.edu.tr

ABSTRACT: This study aimed to determine the soil erosion risk in agricultural areas of Barak Plain (Gaziantep). The magnitude of soil erosion risk was investigated by the application of Revised Universal Soil Loss Equation and Geographic Information Systems and results were displayed as erosion risk maps. From the research area, 14 stations were determined. Soil erosion risk and several physicochemical properties of soils were investigated. The results showed a high erodibility factor and at the same time a very low content of organic matter in the soils of the studied area. This study indicated the necessity of taking more efficient precautions against erosion urgently.

Keywords: Barak plain, K-Factor

INTRODUCTION

Soil erosion in both Turkey and the world causes huge environmental and economic damage, particularly concerning dams [1,2,3,4,5,6,7]. The lack of awareness and knowledge among the farmers increases the erosion hazard [7]. The arable land in Gaziantep Province in southeastern Turkey is cultivated in a conventional way, mostly without applying protective measures are not applied anywhere in Turkey. Therefore, an increase of the hazard of soil erosion can be observed, instead of a decrease [8]. To rise awareness about the threat of soil erosion and to encourage farmers to intensify soil protection measures, this work was accomplished and the results presented to the farmers in the region. After [9] pointed out the important interrelations and close connections between K-factor and content of organic matter, soil type, aggregat class and permeability class, a finding that was confirmed by [10]. After [11]soils with a higher factor of erodibility are more prone to erosion than those with a lower K-factor. The factor of soil erodibility (K-factor) represents the annual soil loss of a certain soil per R-unit on a standard-slope (22 m lenght, 9 % inclination, constant bare fallow). The K-factor is the measure of the soil erodibility and is determined by a number of soil characteristics. Hence, it is an empirically established ratio value expressing

the cumulative effect of all operating soil properties. After [12], the K-factor is derived by calculation of five soil properties: content of silt and fine sand 2-100 µm and soil structure (aggregate class), increasing the factor, and content sand 100-2000 µm, organic matter and permeability, reducing the factor.

MATERIAL AND METHODS

This soil erosion study was conducted at three towns in Gaziantep province (Nizip, Karkamış and Oğuzeli). In the east of the study site, the river Euphrates flows. The soil of the Gaziantep catchment area assemble from 55.38 % Chromic Cambisols, 23.09 % colluvial soils, 8.13 % Cambisols, 7.37 % soils from basaltic parent rock and 1.28 % other soil types such as Regosol, Terra rossa and Terra fusca [13].

Location, Climate, Vegetation and Land use properties of Study Area

The climatic conditions of southeastern Anatolia are distinctly continental with dry and hot summers and cold winters with a low precipitation rate (Tab. 1). Mean annual precipitation is 578.8 mm in Gaziantep, 328.2 mm in Karkamış, and approximately 464 mm in Nizip. Pistachio nuts are frequently cultivated in Gaziantep, as are olives, almonds and partially wine. The natural vegetation mainly consists of grasslands with dwarf shrubs, and to a smaller extent also steppe, garrigue, forest and macchia. Large steppes exist particularly south of Karkamış und Oğuzeli. In the areas of the Nizip, Karkamış and Oğuzeli grow Oak forests ocur, the lowlands are agricultural areas for the production of pistachio, barley and wheat. In Gaziantep Province occur especially the following plants: Alnus sp, Pinus nigra, Cedrus libanii, Cupressus sp., Fagus orientalis, Populus sp., Quercus sp., Juniperus sp., Olea europaea, Arbutus andrachne, Pistachio terebinthus, Styrax officinalis, Euphorbia sp., Paliurus spina-christi, Urtica sp. and Rubus sp. [14].

Table. 1. Mean long term precipitation in Gaziantep Province (1970-2011).

Months (1-12)	1	2	3	4	5	6	7	8	9	10	11	12
Mean temperature (°C)	3.1	4.4	8.4	13.3	18.7	24.1	27.9	27.5	22.9	16.4	9.3	4.8
Mean max. temperature (°C)	8.0	9.6	14.3	19.8	25.7	31.4	35.5	35.5	31.4	24.5	16.0	9.9
Mean min. temperature (°C)	-0.7	0.1	3.3	7.5	12.0	17.1	21.1	21.0	16.4	10.5	4.5	1.0
Mean sunshine (h d-1)	3.5	4.3	5.3	6.5	8.4	10.3	10.5	10.1	8.6	7.1	5.3	3.5
Mean rainy days	12.3	12.2	12.1	10.9	6.9	2.2	0.7	0.5	1.6	6.5	9.0	11.8
Mean amount of precipitation (L m-2)	90.0	82.7	73.6	58.2	29.5	6.7	2.7	2.7	6.2	37.9	68.6	93.0

METHODS

For an appropriate characterisation of the study sites' soils and their susceptibility to soil erosion, the following methods were applied: Colour of soil by use of Munsell Soil Chart [15], pH-value via [16] with Hanna Model (HI 83140 model), electrical conductivity after [17], $CaCO_3$ content by means of Scheibler-method after [18] by the use of Eijkelkamp M1.08.53.D Model calcimeter, organic matter content via [19] , grain size analysis after [20] by means of Retsch model AS 200, aggregate classes after [21] and permeability classes after [22] and K-factor after [10], the RUSLE model after [23]. The GIS analysis was conducted via ERDAS Imagine 8.7, ArcGIS ArcInfo Workstation 10.0 and Microsoft Office. Nitrogen was determined after [24] , Fe, Zn, Mn and Cu after [25] by means of the AAS device, plant available phosphorus (P) after [26] , Potassium (K), Ca and Mg by ASS device after [27]. Statistical analysis was accomplished via SPSS 10.0 for Windows. A total of 14 soil samples were collected at a depth of 30 cm from arable land with an inclination of approximately 10 %. Each sample position was recorded by means of GPS (Magellan 500). Plant communities were recorded and classified on-site.

Determination of K-factor (Eq. 1)

$$K = 2.77 * 10^{-6} * M^{1.14} * (12-OM) + 0.043 * (A-2) + 0.033 * (4-D) \quad \text{(Eq. 1)}$$

with
M = (% silt + % fine sand) * (% silt + % sand (fine sand excluded))
OM = % Organic matter
A = Aggregate stability
D = Permeability class

The soil erodibility factor (K-factor) is classified after [10] (Tab. 2).

Tab. 2 Classification of K-factor [22]

K – Factor	Assessment
K < 0.1	Very low
0.01< K < 0.2	Low
0.2 < K < 0.3	Medium
0.3< K <0.5	High
K >0.5	Very high

RESULTS

Chemical and physical proferties of Soil

For the testet soils, we found pH-values from 7.48 to 7.69 and an electrical conductivity between 0.03 and 0.07 mS cm^{-2}. The soil organic matter was determined as low, ranging from 0.13 to 2.862 %, whereas the CaCO3 content was high. Macronutrients (K, Ca and Mg) and micronutrients (Fe, Cu, Zn, Mn) were determined and evaluated after [25] the Cu-content was measured between 0.95 and 3.74 ppm for all sites, which is considered a sufficent supply (>0.2 ppm). The Fe-content was too low between 0.74 and 1.72 ppm, which means a partly sufficent supply (>1 ppm). The Mn-content of all soils was found sufficient between 1.57 and 7.35 ppm. The Potassium-content of all soils was very high with values between 35 and 72 ppm (>2,56), which was also the case for Mg: the content was determined between 148 and 568 ppm, what is considered very high.

Tab. 3. Soil physical and chemical properties of study site soils

Nr.	pH	% EC	Colour	ΔGMD*	% CaCO3	Ca ppm	K ppm	Mg ppm	Zn ppm	Mn ppm	Fe ppm	Cu ppm	N ppm
	7.56	0.07	5 YR 3/4	2,7	4.5	3298	72	476	1.19	4.98	1.21	2.89	0.084
	7.58	0.03	7.5 YR 5/6	1,09	22.0	4691	43	211	0.61	1.57	0.98	0.95	0.161
	7.51	0.04	5 YR 5/6	1,35	22.0	5201	67	479	0.46	3.21	1.64	2.04	0.033
	7.69	0.04	5 YR 4/6	1,17	22.0	5894	35	223	0.37	3.80	0.74	2.35	0.071
	7.61	0.05	5 YR 4/4	1,04	20.0	3735	63	277	0.88	7.35	1.49	3.74	0.073
	7.62	0.05	7.5 YR 6/4	1,02	21.0	4624	57	148	0.65	5.21	1.14	2.93	0.056
	7.56	0.05	5 YR 4/4	1,13	22.0	4311	62	376	0.6	3.06	1.02	1.93	0.071
	7.57	0.05	7.5 YR 5/4	1,22	22.0	5547	41	178	0.63	4.37	1.18	2.70	0.069
	7.67	0.04	5 YR 5/6	1,23	21.0	5813	48	568	0.30	4.09	1.08	2.47	0.069
	7.56	0.04	10 YR 5/4	1,21	23.0	4946	54	436	0.49	2.73	1.72	1.81	0.07
	7.58	0.04	10 YR 6/3	2,75	21.0	4233	65	332	0.72	2.90	1.10	1.86	0.067
	7.64	0.06	7.5 YR 5/4	1,44	20.0	3996	50	411	0.63	2.46	1.30	1.65	0.046
	7.57	0.06	5 YR 4/4	1,09	23.0	5634	37	546	0.32	2.60	1.61	1.73	0.071
	7.48	0.04	10 YR 7/3	2,1	21.0	3819	69	264	0.69	4.52	1.58	2.76	0.043

ΔGMD* (Aggate stability)

K-Factors of soils in Barak Plain

The K-factors of the soils in the vicinity of Barak Plain were calculated between 0.34and 0.69, which means a high susceptibility to soil erosion for the tested arable land within the RUSLE model [23].

Tab. 4. K-Factors of Barak Plain soils

Soil Nr.	% S*	% Si*	% C*	M	A*	D*	SOM*	K-factor*
	36.87	26.17	36.96	3277.11	1	1	1.86	0.34
	52.02	40.40	7.58	5566.76	1	1	1.30	0.61
	26.79	45.64	27.56	4413.75	1	2	0.13	0.49
	41.78	47.87	10.35	6441.44	1	1	1.56	0.69
	22.22	51.28	26.50	4543.34	1	2	1.50	0.45
	61.68	20.19	18.13	5038.03	1	2	1.56	0.50
	35.56	47.45	16.98	5206.01	2	1	1.37	0.61
	26.48	47.17	26.35	4434.04	1	1	1.56	0.47
	22.51	51.40	26.09	4643.60	1	1	1.04	0.52
	33.66	52.41	13.93	5989.61	1	1	1.30	0.66
	22.30	39.19	38.51	3152.42	1	1	1.17	0.35
	22.35	37.42	40.24	2846.36	3	1	0.72	0.41
	25.06	47.12	27.82	4521.10	3	1	0.52	0.61
	24.69	36.96	38.35	3111.65	3	1	1.04	0.43

A*(aggregate class), D*(permeability class), SOM* (soil organic matter g kg-1), K-factor*(erodibility faktor), S*(Sand), Si*(Silt), C*(Clay)

Soil erosion mapping

The study sites' total surface is 199.886 ha, of which 73.003 ha are Oğuzeli, 31.231 Karkamış and 95.652 ha Nizip region. The GIS erosion maps show, that the study regions are threatened by a similar erosion risk. Particularly the higher elevations are prone to severe soil loss, due to the destroyed vegetation cover. The erosion risk of Karkamış soils was determined low for 89.52 %, medium for 0 %, high for 10.48 % and very high for 0 % (Fig.1).

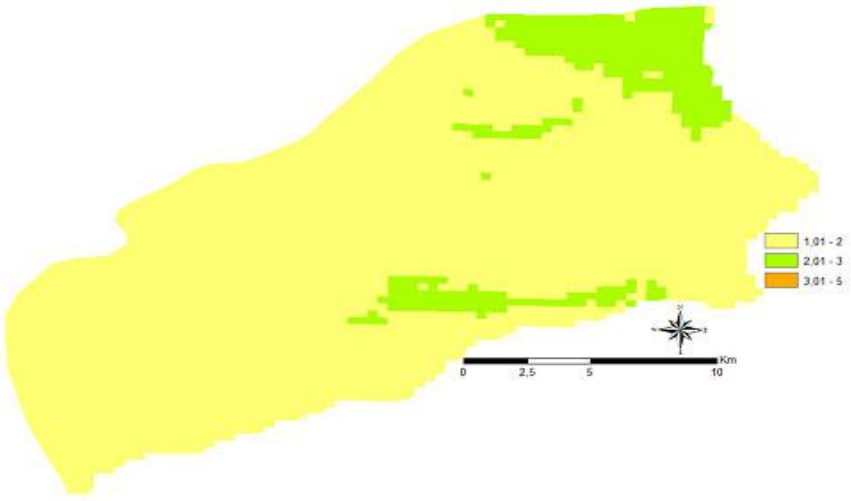

Fig. 1. Erosion risk of Karkamış

The erosion risk of Nizip soils was determined low for 55.54 %, medium for 28.55 %, high for 9.43 % and very high for 6.68 % (Fig.2).

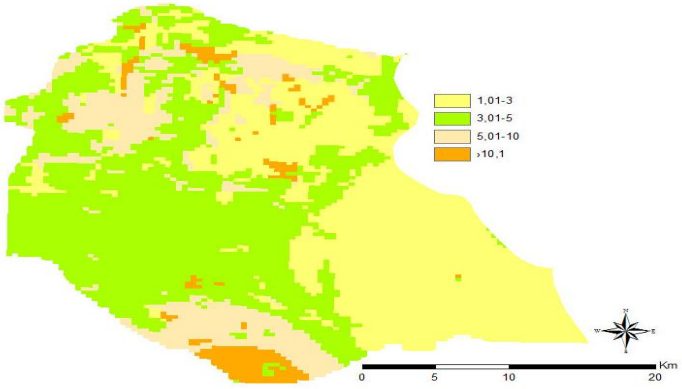

Fig. 2. Erosion risk of Nizip

The erosion risk of Oğuzeli soils was determined low for 42.17 %, medium for 40.18 %, high for 13.74 % and very high for 3.92 % (Fig.3).

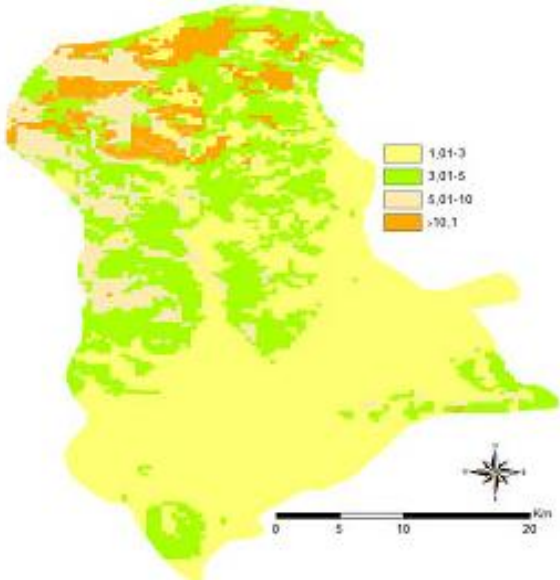

Fig. 3. Erosion risk of Oğuzeli

DISCUSSION AND RECOMMENDATIONS

The results show a high K-factor of the, soils in the study site and at the same time a very low content of organic matter. To increase the content of humus and thus promote and enhance microbiological activity and properties, we suggest organic matter. Furthermore, instead of conventional ploughing, a more shallow working solution should be aspired. Protective measures against soil loss should be applied

as soon as possible, particularly north of the study area. We recommend a close cooperation between farmers and soil scientists for the sake of a proper application of suitable erosion protection: possible means are regular seminars and supervision by experts. Specific topics addressed should be information about crop cultivation and soil treatment, and particularly recent developments of soil conservation. The specific plants growing in that region should be protected and the cultivation encouraged. These plants, which are important in terms of preventing erosion, are distributed in Gaziantep region and can all be recommended to prevent erosion. These plants are perennial ones and widely distributed in meadows, pastures, rocky, stony, pebble, arid slopes, fields and cultivated lands. Especially sloped areas should be vegetated with horizontally developing and creeping plants with different root depths. Intensification and widespread use of these pioneer plants in the region will significantly eradicate erosion problem in the region [14]. Blue-green algae applications to soil may result in an increase in aggregate stability and may provide good protection against erosion [28,29].

ACKNOWLEDGEMENTS

We would like to thank the Gaziantep University for funding the project (BAPB FEF0808) and the department of forestry for providing some data.

REFERENCES

[1]Jarvis, N.J. Gachene, C.K.K., Linner, H. And Mbuvi, J.P., (1997) Soil erosion effect in Highland Central Kenya. Soil Sci. Soc. Am.J., 61:559-564.

[2]Tunç, E. and Schröder, D. (2010a) Vergleichen der Bodenerosion von Landwirtschaftlich Genutzten flöchen in Mittenanatolien und Rheinland-Pfalz. Ege Ünv, Ziraat Fak, Dergisi, 47; 11-20.

[3]Tunç, E. and Schröder, D. (2010b.) Ankara'nın Batısındaki Tarım Topraklarında USLE ile Erozyon Boyutunun Tespiti, Ekoloji Dergisi, Vol: 19: 58-63.

[4]Lal, R. ve Stewart B.A. (1990) Soil degradation, Vol. 11—Advances in Soil Science. New York: Sprin-ger- Verlag.

[5]Djodjic F. and Spännar, M. (2012) Identification of critical source areas for erosion and phosphorus losses in small agricultural catchment in central Sweden. Acta Agriculturae Scandinavica, Section B - Soil & Plant Science Volume 62, pages 229-240.

[6]Tunç, E. and Özkan, A. (2010) Gaziantep'in Tarım Topraklarında Erozyon Sorunu ve Bu Konuda Çiftçi Eğitimi. EÜFBED - Erzincan Üniversitesi Fen Bilimleri Enstitüsü Dergisi Cilt-Sayı: 3-2; 143-153.

[7]Pimentel. D. Harvey, C., Resosudarmo, P., Sinclair, K., Kurz, D., McNair, M., Crist, S. Shpritz, L. Fitton, L. Saffouri, R., Blair, R. (1995) Environmental and economic costs of soil erosion and conservation benefits. Science 267: 1117-1123.

[8]Kirby, P.C. and Mehuys, G.R. (1987) Seasonal Variation of Soil Erodobilities in South Western Quebec, Journal of Soil Water Conservation, 42:211-215.

[9]Schwertmann, U., Vogl ,W., Kainz, M. (1987) Bodenerosion durch Wasser. Vorhersage des Abtrags und Bewertung von Gegenmassnahmen. Stutgart, 86 p.

[10]Morgan, R.P.C. (1985). Soil erosion measurement and soil conservation research in cultivated areas of the UK. Journal of Geography.151:11-20.

[11]Wischmeier, W.H. Smith, D.D. (1978) Predicting Rainfall Erosion Losses Guide to Conservation, Agricultural Handbook 537. Planning, Science and Education Administration. US Dep. of Agriculture, Washington, DC, USA. 58 p.

[12]Anonymous (1992) Gaziantep İli Arazi Varlığı, Tarım ve Köy İşleri Bakanlığı, Köy Hizmetleri Genel Müdürlüğü Yayınları, İl Rapor No: 27 s: 26-28, Ankara.

[13]Tunç, E., Özyazgan, Y., Yayla, F. (2013) Investigation of the Plants Which Can Be Used To Prevent Erosion in Gaziantep Region. Fresenius Environmental Bulletin (FEB) 22, 9a, p.2782-2788.

[14]Munsell Color (2000) Munsell Soil Color Charts, 2000 Revised Washable Edition. Gretagmacbeth, New Windsor, NY.

[15]Schlichting, M., Blume, E. (1966) Bodenkundliches Practium. Verlag Paul Pary, Hamburg and Berlin.

[16]Richards, L.A. (1954) Diagnosis and improvement of saline and alkali soils. US Salinity Lab., US Department of Agriculture Handbook 60. California, USA.

[17]Kretzschmar, R.(1984) Kulturtechnisch- Bodenkundliches Praktikum, Ausgewählte Laboratoriumsmethoden. Eine Einleitung zum selbständigen Arbeiten an Böden.

[18]Allison, L.E. and Moodie, C.D. (1965) Carbonate. In: Black, C.A. [ed.]: Methods of Soil Analysis. Part 2. Chemical and Microbiological Properties, pp. 1379-1396. American Society of Agronomy, Madison.

[19]Schmidt, J. (1996) Entwicklung und Anwendung eines physikalisch begründeten Simulationsmodells für die Erosion geneigter landwirtschaftlicher Landflaechen. Berliner Geographische Abhandlungen, Heft, 61.

[20]Ad-hoc-AG Boden (1982) Bodenkundliche Kartieranleitung. Bundesanstalt für Geowissenschaften und Rohstoffe und Geologische Landesämter in der Bundesrepublik Deutschland (Hrsg.), 3. Auflage, Hannover.

[21]Ad-hoc-AG Boden (1994) Bodenkundliche Kartieranleitung. Bundesanstalt für Geowissenschaften und Rohstoffe und Geologische Landesämter in der Bundesrepublik Deutschland (Hrsg.), 4. Auflage, Hannover.

[22]Renard KG, Laflen JM, Foster GR, Mccool DK (1994) The Revised Universal Soil Loss Equation, In: R. Lal (Editor), Soil Erosion Research Methods, Second edit. St. Lucie Press, Ankeny, 340 p.

[23]Kaçar, B. (1995) Bitki ve Toprağın Kimyasal Analizleri. III. Toprak Analizleri. Ankara Üniversitesi Ziraat Fakültesi Eğitim Araştırma ve Geliştirme Vakfı Yayınları, No: 3, ss 705, Ankara.

[24]Lindsay, W.L. and Norvell, W.A. (1978) Development of a DTPA Soil Test for Zinc, Iron, Manganese and Copper. Soil Sci. Amer. Jour., 42 (3): 421-428.

[25]Olsen, S.R., Cole, C.V., Watanabe, F.S., Dean, L.A. (1954) Estimation of available phosphorus in soil by extraction with sodium bicarbonate. USDA Circ., 939. U.S. Cov. Print Office, Washington D.C.

[26]Jackson, M. (1958) Soil chemical analysis. p. 1-498. Prentice-Hall, Inc. Englewood Cliffs, New Jersey, USA.

[27]Rao, D.L.N., Burns, R.G. (1990) The effect of surface growth of bluegreen algae and bryophytes on some microbiological, biochemical, and physical soil properties. Biol Fertil Soils 9:239-244.

[28]Rogers S.L., Burns R.G. (1994) Changes in aggregate stability, nutrient status, indigenous microbial populations, and seedling emergence, following inoculation of soil with Nostoc muscorum. Biol Fertil Soils. 18:209-215.

[29]Hu, C., Liu, Y., Song, L. and Zhang, D. (2002) Effect of desert soil algae on the stabilization of fine sands. Journal of Applied Phycology 14: 281–292.

A NOVEL APPROACH TO LIFE SPAN PREDICTION OF CONTAINER HOUSES VIA ADAPTIVE NEURO-FUZZY INFERENCE SYSTEM

Nihat ATMACA
Vocational School of Technical Sciences, Gaziantep University, atmaca@gantep.edu.tr

ABSTRACT: Buildings are expected to be long-lived engineered works under usual conditions. In Life Cycle Assessment (LCA) of building analysis, Life Span is one of the most effective parameter. The aim of this study is to make the Life Cycle Assessment analysis of containers and to investigate the relationship between Life Span and consumed energy via Adaptive Neuro-Fuzzy Inference System (ANFIS) approach. The proposed model in the study focused on the construction phase of the containers to estimate total energy use for different life span years. Life span years are chosen between 5-100 years interval. It is found that energy and emission values are decreasing with the increase of life span years in container type houses. The results of the proposed ANFIS modeling approach shows very promising results. According to the results ANFIS approach is a viable tool for Life Span more accurate predictions in LCA studies.

Key words: Life Cycle Assessment, Life Span, Adaptive Neuro-Fuzzy Inference System, Containers

INTRODUCTION

Turkey is located in a very strategic region that is affected by severe natural (earthquakes, floods etc.) and man-made (civil wars) disasters. Recovery works undertaken to eliminate physical, economic, social and environmental losses caused by disasters constitute an important part of the disaster management process. The Disaster and Emergency Management Presidency of Turkey (AFAD) is a governmental organization established in 2009 to take necessary measures for effective emergency management and civil protection nationwide in Turkey. AFAD has prepared a performance indicator for the improvement of recovery capacity between 2013 and 2017 years in Turkey (Table 1) (AFAD, 2012).

Table 1 Performance indicator

Indicator	2013	2014	2015	2016	2017
Capacity of established container cities (person - cumulative)	50,555	50,555	50,555	50,555	50,555
Capacity of stocked containers (person -	19,225	32,870	32,870	32,870	32,870

cumulative)					
Number of personnel trained on recovery processes increased yearly by	58%	58%	58%	58%	58%
Repayment ratio for disaster loans extended to eligible families	40%	45%	50%	55%	60%
Yearly melting rate of increasing disaster housing stock	40%	40%	40%	40%	40%
Improving the damage assessment process	20%	20%	20%	20%	20%
Realization ratio according to number of total disaster houses in the annual programme (17,535 houses in the programme at start of 2013)	40%	45%	50%	55%	60%
Ratio of cases lost in lawsuits related to Law no.7269 finalized within the year decreased by (based on 2012 figures)	5%	10%	15%	20%	25%

According to the AFAD statistics, there is a continuing need for disaster housing stocks. The use of energy for the container houses have been increasing and can be expected to increase in the future. Therefore, the choice of the housing type is an important area for reducing energy requirements and greenhouse gas emissions.

LCA methods have been used for environmental evaluation in many industries and by many researchers to assist with decision-making for environment-related strategies and to reduce buildings' life cycle environmental impacts last decades (Singh, Berghorn, Joshi & Syal, 2011; Buyle, Braet & Audenaert, 2013).

According to ISO 14040, LCA is the investigation and evaluation of environmental impacts of a given product, system or service, over its entire life cycle.

A simplified version of LCA, life cycle energy analysis (LCEA) is used to assess the environmental impact of buildings. It focuses only on the evaluation of energy inputs for different phases of the life cycle. This methodology is applied to several studies found in the literature (Ramesh, Prakash & Shukla, 2010).

In addition to LCEA, Life Cycle Carbon Emissions Assessment ($LCCO_2A$) is used for evaluating the CO_2 emissions as an output over the whole life cycle of a building. The approach considers all the carbon- equivalent emission output from a building over different phases of its life cycle (Atmaca, 2016).

Container houses play a significant role in consumption of energy resources especially after disasters. Thus, container type housing is an important area to

represent a major opportunity for reducing energy requirements and greenhouse gas emissions. This paper is the first study predicting Life Span of containers in order to make LCEA.

Fay et al. (2000) examined the primary energy use of a detached house in Melbourne, Australia. LCEA over lifespans of 0, 25, 50, 75 and 100 years were carried out for the base case and then with added insulation. Total energy consumption of the building is calculated to be 76 GJ/m^2 in 50 years of life span.

Bastos et al. (2014) showed the linkage between building design, energy use and GHG emissions. The linkage is dependent on and sensitive to climate and sociodemographic characteristics that are geographically and culturally variable. It was also shown that larger buildings have lower life cycle energy requirements and GHG emissions on a square meter basis and reverse pattern on a per person basis.

Atmaca (2016) investigated the total energy use and CO_2 emissions over 15 and 25 year lifespans for container and prefabricated houses respectively. It was concluded that operation phase energy has a major share in both LCEA and $LCCO_2$ on a per meter square basis.

There are some studies about the final energy consumption of residential buildings in Turkey. However, the studies about the life cycle energy consumption and environmental effects of container houses are limited in number and scope in literature. Meanwhile, there is currently very few studies about the final energy consumption of residential buildings in Turkey (Atmaca and Atmaca 2015). Complex real-world problems may require intelligent systems that possess human-like expertise within a specific domain, adapt themselves to changing environments, and be able to explain how they make decisions or take actions (Donald, 1986). Various artificial intelligence (AI) techniques (fuzzy logic and neural networks) have been developed and used in industrial applications (Liebowitz, 1990). This study uses such an attempt by using ANFIS to predict the Life Span of containers. The data obtained from the LCA analyses (Atmaca, 2016) is used to test and train ANFIS. The input variables used in ANFIS to estimate the Life Span of container are; Construction phase embodied energy and used area in Container Houses. Numerical results reveal a good agreement among the test, fuzzy and ANFIS results.

METHODS

Adaptive Neuro-Fuzzy Inference System (ANFIS)

Fuzzy modeling (Jang et al. 1997) is an emerging branch of system identification. The model deals with the construction of a fuzzy inference system or 'fuzzy model'. By the way, prediction and explanation of the behavior of an unknown

system or parameter can be described by a set of sample data. A fuzzy-inference system employing fuzzy 'if–then rules' can model the qualitative aspects of human knowledge and reasoning processes without employing precise quantitative analyses. The fuzzy modeling or fuzzy identification studies carried out systematically by Takagi and Sugeno (1985).

The implementation of Fuzzy Logic (FL) to real applications considers the following steps (Bai et al. 2006):

(1) Fuzzification, which requires conversion of classical data or crisp data into fuzzy data or membership functions (MFs),
(2) Fuzzy inference process, which connects MFs with the fuzzy rules to derive the fuzzy output,
and
(3) Defuzzification, which computes each associated output.

Fuzzy systems can be connected with neural networks to form Neuro-Fuzzy systems which reveal advantages of both approaches. Neuro-fuzzy systems combine the FL's natural language description and NN's learning properties. Various Neuro-Fuzzy systems have been developed that are known in the literature under short names. Adaptive network-based fuzzy inference system (ANFIS) developed by Jang (Jang et al. 1997) is one of the Neuro-fuzzy systems which allows the fuzzy systems to learn the parameters using adaptive backpropagation learning algorithm (Rutkowski 2004).

Three types of fuzzy inference systems (FISs) have been widely employed in various applications:

Mamdani,
Sugeno,
Tsukamoto

The differences between these three fuzzy inference systems are due to the consequents of their fuzzy rules, and thus their aggregation and defuzzification procedures differ accordingly (Jang et al. 1997).

The Sugeno FIS is used in present study. Each rule is defined as a linear combination of input variables in a Sugeno FIS. The corresponding final output of the fuzzy model is simply the weighted average of each rule's output. A Sugeno FIS consisting of two input variables x and y, for example, a one output variable f will lead to two fuzzy rules:

Rule 1: If x is A1, y is B1 then $f1 = p1x + q1y + r1$
Rule 2: If x is A2, y is B2 then $f2 = p2x + q2y + r2$

where pi , qi and ri are the consequent parameters of the ith rule. Ai , Bi and Ci are the linguistic labels which are represented by fuzzy sets shown in Figure 1.

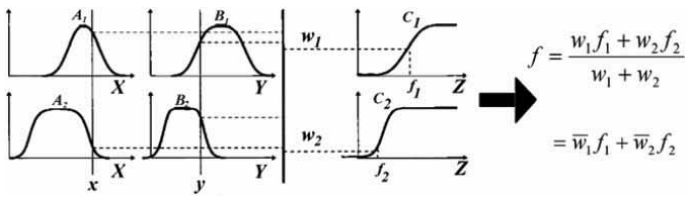

Figure 1. The Sugeno Fuzzy Model (Jang et al. 1997).

In the present study, MATLAB FL Toolbox is used for the ANFIS modelling process. Various types of MFs such as Gaussian, Gaussian combination, generalized bell-shaped, triangular-shaped and trapezoidal-shaped are used.

Life Cycle Assessment Analysis

The elementary concept of LCA is to calculate the environmental impacts of a product over different life cycle stages. LCA evaluates all the resources inputs, including energy, water and materials, and environmental loadings including CO_2 emissions and wastes of a building during different phases of the life cycle. Mathematically;

$$I = I_{Extraction} + I_{Manufacture} + I_{Onsite} + I_{Operation} + I_{Demolition} + I_{Recycling} + I_{Disposal}$$

Where I represents the life cycle environmental impact, and Ij represents the environmental impacts of jth building phase.

LCEA focuses on energy inputs to a system and $LCCO_2A$ focuses on the CO_2 equivalent emissions released from a system (Fig.3).

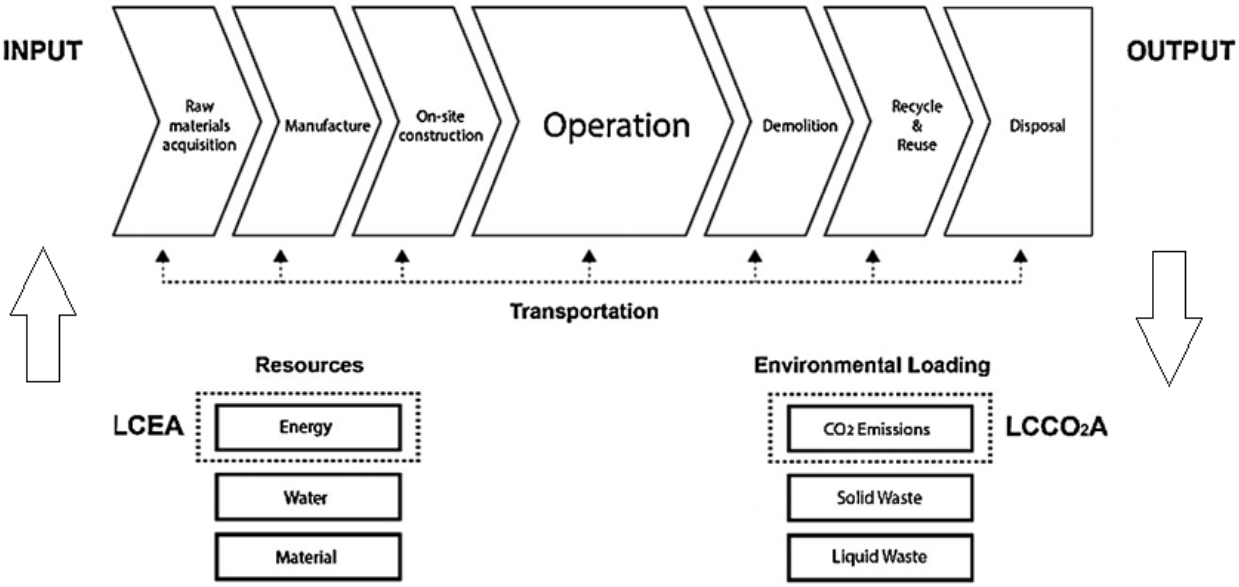

Figure 2. Basic models of LCEA and $LCCO_2A$ (Atmaca &Atmaca, 2015).

Construction, operation and demolition of buildings consumes large amount of energy and produces lots of CO_2 emissions. Predictions over energy consumption during operation phase of the building life cycles and assumptions about the end of the life span of the houses are highly uncertain. Therefore, only the construction phase is used for the energy analysis with different life span years by using ANFIS modelling process.

Technical specifications and the floor plan of the CH are presented in Table 2. The typical CH has a gross area of 20, 21 and 22 m^2 with one story, two rooms and a WC inside it.

Table 2.Technical specifications of CH

Specifications	CH
Foundation	20 cm concrete with 6x150x150 mm mesh reinforcement
Structural System	Steel profiles and wall panels
Exterior And Interior Walls	35 mm thickness sandwich plasterboard panels
Floors	16 mm thickness precast concrete panels and 3 mm PVC coatings
Roof Covering	Galvanized roller steel sheets, OSB, 80 mm thickness glass-wool
Doors	900*2100 mm steel framed for exterior door and 800*2100 mm PVC framed for interior doors
Windows	100*110 mm PVC framed with single 4 mm single glazing.
Exterior surface coatings	Sandwich plasterboard panels

Construction phase analysis

Construction phase analysis includes embodied energy (EE) and CO_2 emissions analysis. EE is defined as the total primary energy (MJ) required by the building materials during manufacturing phase (Hammond & Jones 2008).

In this study, Inventory of Carbon and Energy (ICE) Version 2.0 (Hammond& Jones 2011) is used for the calculation of primary energy requirements. The ICE includes the embodied energy, carbon and GHG (measured in grams of CO_2 equivalent, g CO_2-eq) for a large number of materials. Some important criteria were applied for the selection of energy values for the individual materials incorporated into the ICE database. This ensures the consistency of data within the inventory. One of the applied criteria is about the compliance of data with approved methodologies and standards (ISO 14040/ 44).

Table 3 Embodied energy for different types of building materials

Type of the building materials	Embodied energy

	intensity (MJ/kg)*
Concrete	0.5–1.6
Galvanized steel	35.8–39
Polymer vinly siding	11.8–120
Precast concrete element	2
Wood	9.1-14.2
Thermal and acoustic insulation	3–45
Plastic, rubber and polymer	67.5–116
Purified fly ash (PFA)	<0.1
Stainless steel	51.5–56.7
Plaster, render and screed	1.4–1.8
Reinforcing bar and structural steel	9.9–35

* Intensity values were extracted from ICE.

Life Span Prediction

Building life span is a very important variable in LCA calculations. The container house type LCA analysis with different Life Span years have been carried out. Among the analysis result database, 17 tests were used as test set and the remaining 61 tests as training set for training. The proposed ANFIS model is based on the output MF is chosen as the simplest function available which is a constant value. The structure of the ANFIS model is shown in Figure 3.

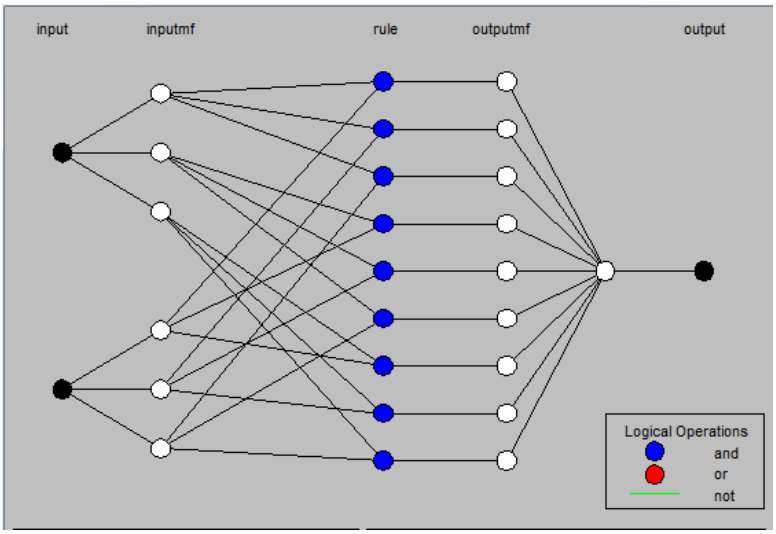

Figure 3 ANFIS Model Structure

The fuzzy inference diagram of the proposed ANFIS model is shown in Figure 4. The initial and final MFs for inputs are presented in Figure 5. The input and output surface of the ANFIS model is given in Figure 6.

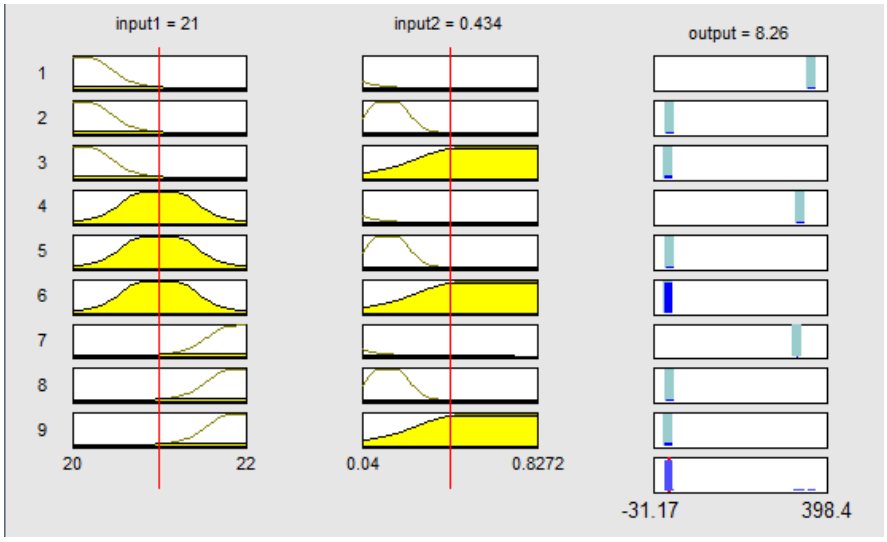

Figure 4 Fuzzy inference diagram of ANFIS model.

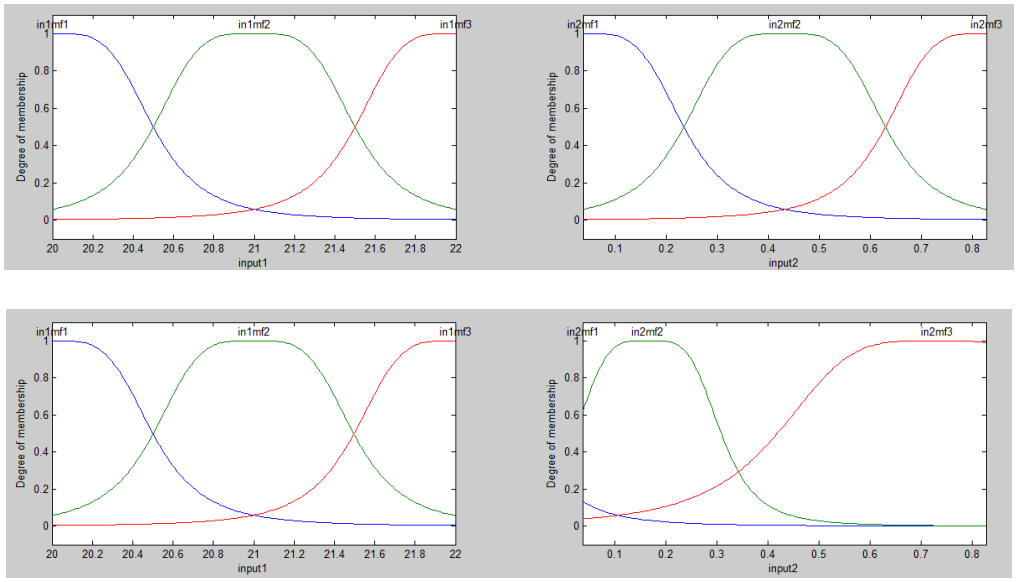

Figure 5 Initial and Final Membership Functions of Inputs

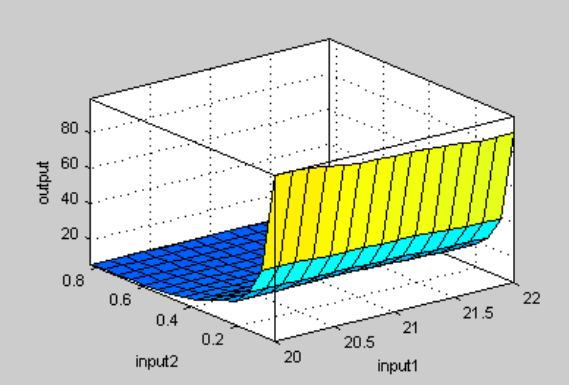

Figure 6 Output Surface of ANFIS Model

RESULTS AND FINDINGS

Life cycle analysis of container housings involves many assumptions, simplifications and uncertainties. The materials used in construction, life span, location and climatic conditions and building data of the houses has the potential to vary the findings of this study.

In Life Cycle Assessment (LCA) of building analysis, Life Span is one of the most effective parameter. The accurate prediction of Life Span has crucial importance in LCA methods. In this context, alternative methods such as soft computing techniques can be used to overcome this difficulty. This study is a pioneer work that search into the capability of neuro-fuzzy (NF) approach for the prediction of Life Span of the container houses. The actual and operational data are considered in the study. Among the 78 total data sets, 17 datas are used as test and the remaining 61 datas are used as training data sets. Sugeno type of FIS is used where each rule is defined as a linear combination of two input variables. The corresponding final output of the fuzzy model is simply the weighted average of each rule's output. The aim is to construct the ANFIS model fitting those values within minimum error for independent input variables. The results of the study show that the energy values are decreasing with increasing Life Span years (Figure 6). The rapid decrease is observed in first 5 and 10 years. The results of the ANFIS has quite satisfactory for future analyses.

CONCLUSIONS

Life Cycle Energy analysis of container houses constructed in Turkey are presented for different Life Span years. The construction phase was used for the analyses. EE and area of the houses are chosen as inputs. Fuzzy-expert rules (IF–THEN rules), membership functions and defuzzification methods are used to eliminate the complexity of the prediction of Life Span. The ANFIS approach generates rules between each input and output. The results of the proposed ANFIS

model are observed to be quite accurate predictions. The outcomes of this study are quite satisfactory which may serve Neuro-Fuzzy approach to be used in LCA applications.

RECOMMENDATIONS

Further studies are needed to investigate more about the use of more comprehensive LCA methods. Hybrid analysis is generally considered the preferred approach for EE analysis due to its systemic completeness and use of reliable data. I–O-based hybrid analysis combines process data and I–O data to process-based hybrid analysis. EE must be considered over the whole life of the container housing Embodied Energy values. The EE values can be reduced with a careful consideration on the design of systems and selection of appropriate building material. The lack of sufficient databases in building LCA area is the most important issue of Turkey. More reliable and accurate estimates can be obtained with a wide range of databases in ANFIS modelling analyses.

REFERENCES

Adalberth K (1997) Energy use during the life cycle of buildings: a method. Building and Environment 32 (4): 317–320.

AFAD (2012) Republic of Turkey Prime Ministry Disaster and Emergency Management Presidency 2013-2017 Strategic Plan AFAD Publication from https://www.afad.gov.tr/upload/Node/2584/files/Afad_Strtjk_web_en_son.pdf.

Atmaca A and Atmaca N (2015) Life cycle energy (LCEA) and carbon dioxide emissions (LCCO2A) assessment of two residential buildings in Gaziantep, Turkey. Energy and Buildings 102: 417-431.

Atmaca N (2016) Life cycle assessment of post-disaster temporary housings in Turkey. Building Research& Information, http://dx.doi.org/10.1080/09613218.2015.1127116.

Bai,Y., Zhuang, H., andWang, D. (2006) Advanced fuzzy logic technologies in industrial applications. Springer.

Bastos J, Batterman SA and Freire F (2014) Life-cycle energy and greenhouse gas analysis of three building types in a residential area in Lisbon. Energy and Buildings 69: 344–353.

Buyle M, Braet J and Audenaert A (2013) Life cycle assessment in the construction sector: a review. Renewable& Sustainable Energy Reviews 26: 379–88.

Donald A.W. (1986) A Guide to Expert Systems, (Addison-Wesley: Reading, MA).
Fay R, Treloar G and Iyer-Raniga U (2000) Life-cycle energy analysis of buildings: a case study. Building Research and Information 28 (1): 31–41.

Liebowitz, J. (1990) The Dynamics of Decision Support System and Expert System, (The Dryden Press: Orlando).

Hammond G and Jones C(2008) Inventory of Carbon and Energy, Version 1.6 Sustainable Energy Research Team (SERT), Department of Mechanical Engineering, University of Bath, UK.

Hammond G and Jones C(2011). Inventory of Carbon and Energy, Version 2.0 Sustainable Energy Research Team (SERT), Department of Mechanical Engineering, University of Bath, UK.

Jang, J.S.R., Sun, C.T. and Mizutani, E. (1997) Neuro-Fuzzy and Soft Computing: a Computational Approach to Learning and Machine Intelligence, (Prentice-Hall International: London).

Rutkowski, L. (2004). Flexible neuro-fuzzy systems: structures, learning and performance evaluation. Kluwer Academic Publishers.

Singh, A., Berghorn,G., Joshi, S.& Syal, M. (2011). Review of life-cycle assessment applications in building construction. Journal of Architectural Engineering, 1, 15–23.

Takagi, T. and Sugeno M. (1985) Fuzzy identification of systems and its applications to modeling and control. IEEE Trans. Syst. Man. Cybern., 15, 116–132.

THE EFFECTS OF LIFE SPAN ON ENERGY CONSUMPTION AND CO_2 EMISSIONS OF CONTAINER HOUSES

Adem ATMACA
Department of Energy Systems Engineering, Gaziantep University, aatmaca@gantep.edu.tr

ABSTRACT: Life span is an important variable in Life Cycle Assessment of buildings. The aim of this study is to make the Life Cycle Assessment (LCA) analysis of containers and to investigate the relationship between life span and consumed energy with CO_2 emission values. The proposed model in the study focused on the construction phase of the containers to estimate total energy use and CO_2 emissions for different life span years. Life span years are chosen between 5-40 years interval. Energy efficiency and emission parameters are defined for the construction per square meter. It is found that energy and emission values are decreasing with the increase of life span years in container type houses.

Keywords: Life Cycle Assessment, Life span, Energy and CO_2 consumption, Containers

INTRODUCTION

Turkey is in the top rankings in the world with regard to people affected in natural and man-made disasters. Recovery works undertaken to eliminate physical, economic, social and environmental losses caused by disasters constitute an important part of the disaster management process. AFAD has prepared a performance indicator for the improvement of recovery capacity between 2013 and 2017 years in Turkey (Table 1) (AFAD, 2012).

Table 1 Performance indicator

Indicator	2013	2014	2015	2016	2017
Capacity of established container cities (person - cumulative)	50,555	50,555	50,555	50,555	50,555
Capacity of stocked containers (person - cumulative)	19,225	32,870	32,870	32,870	32,870
Number of personnel trained on recovery processes increased yearly by	58%	58%	58%	58%	58%
Repayment ratio for disaster loans extended to	40%	45%	50%	55%	60%

eligible families					
Yearly melting rate of increasing disaster housing stock	40%	40%	40%	40%	40%
Improving the damage assessment process	20%	20%	20%	20%	20%
Realization ratio according to number of total disaster houses in the annual programme (17,535 houses in the programme at start of 2013)	40%	45%	50%	55%	60%
Ratio of cases lost in lawsuits related to Law no.7269 finalized within the year decreased by (based on 2012 figures)	5%	10%	15%	20%	25%

Table 2 shows that there is a continuing need for disaster housing stocks. The use of energy for the container houses have been increasing and can be expected to increase in the future. Therefore, container housing is an alternative area for reducing energy requirements and greenhouse gas emissions.

LCA methods have been used for environmental evaluation in many industries for a long time. The methods have been increasingly used by researchers to assist with decision-making for environment-related strategies and to reduce buildings' life cycle environmental impacts (Buyle et al. 2013).

The studies about building LCA methods mostly started after Adalberth (1997). He analysed the life cycle energy use of the construction, use and end-of-life phases of three dwellings in Sweden. It was concluded that, operating energy has a major share (80–90%), followed by embodied energy (10–20%), whereas demolition and other process energy have negligible or little share in LCEA.

Fay et al. (2000) examined the primary energy use of a detached house in Melbourne, Australia. They took advantage of alternative designs using additional insulation and found that the addition of higher levels of insulation in Australia paid back its initial EE in life-cycle energy terms in around 12 years. LCEA over lifespans of 0, 25, 50, 75 and 100 years were carried out for the base case and then with added insulation. Total energy consumption of the building is calculated to be 76 GJ/m^2 in 50 years of life span. The additional insulation decreased the total energy of the house by 3.4 GJ/m^2 of floor area.

Bastos et al. (2014) showed the linkage between building design, energy use and GHG emissions. The linkage is dependent on and sensitive to climate and sociodemographic characteristics that are geographically and culturally variable. It was also shown that larger buildings have lower life cycle energy requirements

and GHG emissions on a square meter basis and reverse pattern on a per person basis.

Atmaca (2016) investigated the total energy use and CO_2 emissions over 15 and 25 year lifespans for container and prefabricated houses respectively. It was concluded that operation phase energy has a major share in both LCEA and LCCO2 on a per meter square basis.

There are also some research projects which have underlined the importance of post-disaster temporary and permanent housing in order to improve the outcomes of reuse and recycle housing projects. Arslan (2007) showed the minimum energy usage for construction should be kept for accelerating the reconstruction of the region and forming a sustainable community, which maintains itself socially, environmentally and economically over time.

There are some studies about the final energy consumption of residential buildings in Turkey. However, the studies about the life cycle energy consumption and environmental effects of container houses are limited in number and scope in literature (Atmaca, 2016). Meanwhile, there is currently very few studies about the final energy consumption of residential buildings in Turkey (Atmaca and Atmaca 2015).

The aim of this study is to make the Life Cycle Assessment analysis of containers and to investigate the relationship between life span and consumed energy with CO_2 emission values.

METHODS

Construction, operation and demolition of buildings consumes large amount of energy and produces lots of CO_2 emissions. Predictions over energy consumption during operation phase of the building life cycles and assumptions about the end of the life span of the houses are highly uncertain. Therefore, the construction phase is used for the energy and CO_2 emission analysis with different life span years in this study.

A typical container house analysed to represent the majority of the houses constructed after an unexpected disaster or natural hazard. Technical specifications of the CH are presented in Table 2. The typical CH has a gross area of 21 m^2 with one story, two rooms and a WC inside it (Figure 1).

Construction phase analysis

Construction phase analysis has two main analysis. It includes embodied energy (EE) and CO_2 emissions analysis. EE is defined as the total primary energy (MJ) required by the building materials during manufacturing phase (Hammond &

Jones 2008). Energy content of all the materials used in the building and technical installations, and energy incurred at the time of new construction and renovation of the building.

In this study, Inventory of Carbon and Energy (ICE) Version 2.0 (Hammond& Jones 2011) is used for the calculation of primary energy requirements and greenhouse gas emissions. The ICE includes the embodied energy, carbon and GHG (measured in grams of CO_2 equivalent, g CO_2-eq) for a large number of materials. Some important criteria were applied for the selection of energy and carbon values for the individual materials incorporated into the ICE database. This ensures the consistency of data within the inventory. One of the applied criteria is about the compliance of data with approved methodologies and standards (ISO 14040/ 44).

LCCO$_2$A considers all the carbon equivalent emission output from a building over different phases of its life cycle. The "Embodied GHG" (EGHG) emissions comprise the GHG emissions from the extraction of raw materials to the building site. In the ICE, the term "embodied carbon" is used for both carbon and GHG emissions. Table 3 (Atmaca, 2016) shows the embodied energy and CO_2 intensities of some building materials.

Table 2.Technical specifications of CH

Specifications	CH
Foundation	20 cm concrete with 6x150x150 mm mesh reinforcement
Structural System	Steel profiles and wall panels
Exterior And Interior Walls	35 mm thickness sandwich plasterboard panels
Floors	16 mm thickness precast concrete panels and 3 mm PVC coatings
Roof Covering	Galvanized roller steel sheets, OSB, 80 mm thickness glass-wool
Doors	900*2100 mm steel framed for exterior door 800*2100 mm PVC framed for interior doors
Windows	100*110 mm PVC framed with single 4 mm single glazing.
Exterior surface coatings	Sandwich plasterboard panels

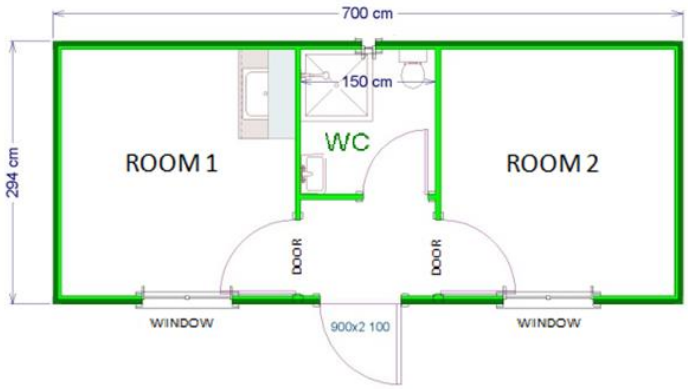

Figure 1. Floor Plan of CH (Atmaca, 2016).

Table 3 Embodied energy and CO_2 intensity ranges for different types of building materials

Type of the building materials	Embodied energy intensity (MJ/kg)*	CO_2 intensity (kg CO_2-eq /kg)*
Concrete	0.5–1.6	0.05–5.15
Galvanized steel	35.8–39	2.82
Polymer vinly siding	11.8–120	2.29
Precast concrete element	2	0.22
Wood	9.1-14.2	0.3–1.12
Thermal and acoustic insulation	3–45	0.15–1.86
Plastic, rubber and polymer	67.5–116	2.2–16.2
Purified fly ash (PFA)	<0.1	0.01
Stainless steel	51.5–56.7	6.15
Plaster, render and screed	1.4–1.8	0.12–0.16
Reinforcing bar and structural steel	9.9–35	1.72–2.82

* Intensity values were extracted from ICE.

The following assumptions were made during the LCA energy and CO_2 emission calculations:

Standard building construction methods and materials were assumed to be the same over the building life cycles.

The building design and materials were obtained mainly from original project documents.

Energy mix and intensities were considered constant over the building life cycles.

The service lives for the structural components were assumed to be equal to the service life of the house.

It was assumed that all final product manufacturing took place around the city and an average occupancy of 4 persons per container housing unit.

Finally, some environmental qualities such as indoor air quality are not included and environmental impacts were assumed to be constant over time in the analysis.

Life Span Prediction

Building life span is a variable and it is too difficult to predict. Temporary housing where optimum conditions are provided in which people can carry on their household daily activities until they move in the permanent housings. The permanent housings is a complex and time consuming process according to the size of the disaster. Therefore the life cycle of the container housing types were chosen between 5-40 years (Table 4).

Table 4 Energy and CO_2 values with different Life Spans

YEARS	ENERGY (GJ/(m^2-year))	CO_2 VALUES(kg CO^2/(m^2-year))
5	0.79	61.16
10	0.39	30.58
15	0.26	20.39
20	0.20	15.29
25	0.16	12.23
30	0.13	10.19
35	0.11	8.74
40	0.10	7.65

It can be clearly seen that the energy and emission values are decreasing with the increase of life span years in container type houses. If we show the results in a different graphical representation we can see a drastic change between 5-10 years (Figures 2).

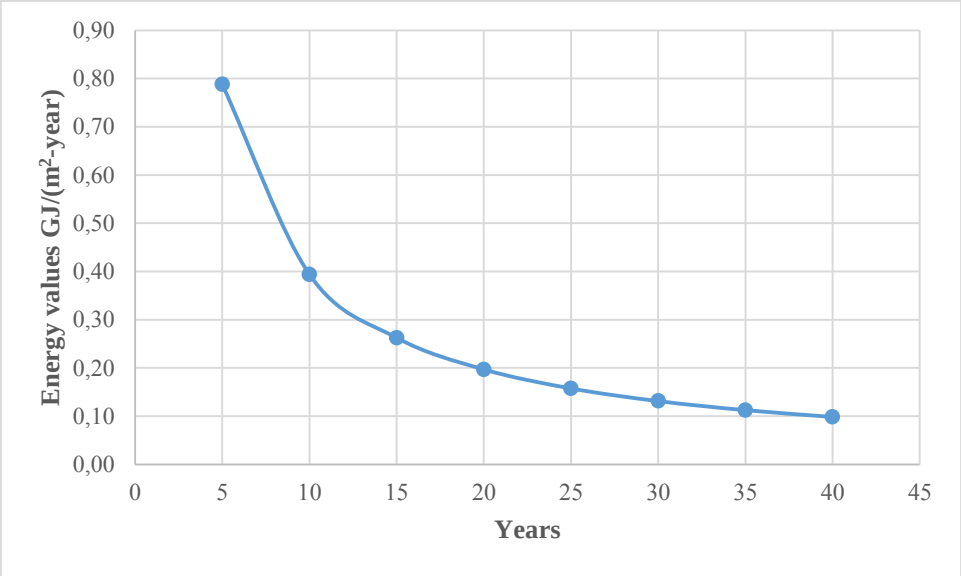

Figure 2 Energy values with different Life Spans

RESULTS AND FINDINGS

Life cycle analysis of container housings involves many assumptions, simplifications and uncertainties. The materials used in construction, life span, location and climatic conditions and building data of the houses will influence 'Cumulative Energy Demand' (CED) that is used to determine and compare the energy intensity of the houses and variations in any of these factors has the potential to vary the findings of this study.

EE must be considered over the whole life of the container housings. EE values can be reduced with a careful consideration on the design of systems and selection of appropriate building material. The results of the study show that the energy and CO_2 emission values are steadily decreasing. The rapid decrease is between 5-10 years (%50).

CONCLUSION

Life Cycle Energy analysis and Life Cycle CO_2 analysis of container houses constructed in disaster areas in Turkey are presented for different life span years. The construction phase was used for the analyses. The energy and CO_2 emission values are decreasing %50 after 5-10 years therefore, the time to make permanent housing should be chosen in this time interval. The results of the study show that for a container house to perform efficiently in terms of energy and CO_2 emissions, material selection and application of insulation and recycling facilities are important considerations. Besides that the use of area and occupancy-based

functional units can give us quite interesting and important information about the life cycle analyses of container houses.

RECOMMENDATIONS

Further studies are needed to investigate more about the use of more comprehensive LCA methods. Hybrid analysis is generally considered the preferred approach for EE analysis due to its systemic completeness and use of reliable data. I–O-based hybrid analysis combines process data and I–O data to process-based hybrid analysis. The specific and wide range of data library for temporary housings may give a change to accurate prediction of the Life Span of Container houses.

REFERENCES

Adalberth K (1997) Energy use during the life cycle of buildings: a method. Building and Environment 32 (4): 317–320.

AFAD (2012) Republic of Turkey Prime Ministry Disaster and Emergency Management Presidency 2013-2017 Strategic Plan AFAD Publication from https://www.afad.gov.tr/upload/Node/2584/files/Afad_Strtjk_web_en_son.pdf.

Arslan H (2007) Re-design, re-use and recycle of temporary houses. Building and Environment 42: 400-406.

Atmaca A and Atmaca N (2015) Life cycle energy (LCEA) and carbon dioxide emissions (LCCO2A) assessment of two residential buildings in Gaziantep, Turkey. Energy and Buildings 102: 417-431.

Atmaca N (2016) Life cycle assessment of post-disaster temporary housings in Turkey. Building Research& Information, http://dx.doi.org/10.1080/09613218.2015.1127116.

Bastos J, Batterman SA and Freire F (2014) Life-cycle energy and greenhouse gas analysis of three building types in a residential area in Lisbon. Energy and Buildings 69: 344–353.

Buyle M,Braet J and Audenaert A (2013)Life cycle assessment in the construction sector: a review. Renewable& Sustainable Energy Reviews 26: 379–88.

Fay R, Treloar G and Iyer-Raniga U (2000) Life-cycle energy analysis of buildings: a case study. Building Research and Information 28 (1): 31–41.

Hammond G and Jones C(2008) Inventory of Carbon and Energy, Version 1.6 Sustainable Energy Research Team (SERT), Department of Mechanical Engineering, University of Bath, UK.

Hammond G and Jones C(2011). Inventory of Carbon and Energy, Version 2.0 Sustainable Energy Research Team (SERT), Department of Mechanical Engineering, University of Bath, UK.